2019•2020

Faculteit Industriële ingenieurswetenschappen

master in de industriële wetenschappen: biochemie

# Masterthesis

# Photodegradation of diclofenac in the first generation of translucent monoliths


PROMOTOR :

Prof. dr. ir. Mumin Enis LEBLEBICI

PROMOTOR :

ing. Mathias JACOBS

Lotte Thys


Scriptie ingediend tot het behalen van de graad van master in de industriële wetenschappen: biochemie

Gezamenlijke opleiding UHasselt en KU Leuven

2019•2020

Faculteit Industriële ingenieurswetenschappen

**master in de industriële wetenschappen: biochemie**

# Masterthesis

## Photodegradation of diclofenac in the first generation of translucent monoliths

**PROMOTOR :**

Prof. dr. ir. Mumin Enis LEBLEBICI

**PROMOTOR :**

ing. Mathias JACOBS


**Lotte Thys**

**Scriptie ingediend tot het behalen van de graad van master in de industriële wetenschappen: biochemie**


UHASSELT

KU LEUVEN

*Deze masterproef werd geschreven tijdens de COVID-19 crisis in 2020. Deze wereldwijde gezondheidscrisis heeft mogelijk een impact gehad op de opdracht, de onderzoekshandelingen en de onderzoeksresultaten.*

# Acknowledgements

This master's thesis forms the final assessment criterion within the framework of the Master program in Biochemical Engineering Technology at Hasselt University in association with KU Leuven. I chose this topic because I am very interested in the pharmaceutical sector. Also, this project is a more chemical oriented research but still linked to the biochemistry by means of the pharmaceutical components. So, this will increase my knowledge within the chemical aspect.

Firstly, I want to thank Prof. dr. ir. Leen Thomassen and Prof. dr. ir. Jozefien De Keyzer. They made it possible for me to do my internship at *Centrum for Industrial Process Technology* (CIPT) laboratory. Here, I was given the opportunity to carry out all the necessary experiments on my own. I also want to thank them to keep us updated during the uncertain period of COVID-19.

Next, I would like to thank my supervisor ing. Mathias Jacobs for the excellent guidance during my internship and while writing my thesis. During the experiments I could always contact ing. Mathias Jacobs for the necessary information. He helped me to solve problems in a correct way. Further, he was also the person I could turn to with all my questions and who always checked and corrected my thesis. The feedback encouraged and helped me enormously to rework and adjust my thesis where necessary. His way of working gave me self-confidence to carry out the tests correctly and to dare to come up with new ideas myself. Also, I want to thank Prof. dr. ir. Mumin Enis Leblebici for the proper follow-up of my internship and guidance during the writing of the thesis. His remarks also helped me enormously to finish this thesis.

Prof. dr. Jeroen Lievens is the following person I want to thank. He gave us all the necessary information to write a scientific thesis. I could always mail him for requisite information, and he was very flexible during the period of COVID-19. I would also like to thank him for checking our trial design, abstract and poster.

As mentioned, I got the opportunity to work on my own. This has given me a good view of the work environment in the research. I would like to thank my fellow students, who also did an internship at the CIPT laboratory. I could always turn to them with questions and they always gave me wise advice. I would also like to thank the other PhD students of the research group. I could contact them whenever I came across a problem. Thanks to them I have gained a lot of experience.

Finally, I want to thank my parents. They gave me the opportunity to start these studies. They supported me not only during the internship but throughout the entire training. Their encouragement gave me the energy at the right time to complete my training.

# Table of content

# List of tables

# List of figures

# Glossary

| | |
|---|---|
| AOP | Advanced oxidation process |
| CFD | Computational fluid dynamics |
| CIPT | Centrum for Industrial Process Technology |
| COD | Chemical oxygen demand |
| DCF | Diclofenac |
| DF | Dilution factor |
| DPA | 9,10-diphenylanthracene |
| FAM | Finite analytic method |
| FDM | Fused deposition modeling |
| HPLC | High pressure liquid chromatography |
| LED | Light-emitting diode |
| PNEC | Predicted no effect concentration |
| PSTY | Photochemical space-time yield |
| ROS | Reactive oxygen species |
| RSD | Relative standard deviation |
| SLA | Stereolithography apparatus |
| STY | Space-time yield |
| UV | Ultraviolet |
| VIS | Visible |

# Abstract in English

The pharmaceutical diclofenac provides effective treatment for pain and inflammatory diseases. However, after administration, the medication is not fully metabolized and ends up in the wastewater with its metabolites. After a regular water treatment, diclofenac is still present in the effluent in concentrations that exceed the *Predicted No Effect Concentration*. The aim of this master's thesis was to degrade diclofenac with photochemistry in a scalable micro-flow reactor, a translucent monolith. This reactor consists of small channels placed parallel next to each other and was used because of its high productivity and energy efficiency.

First, experiments were performed in batch reactors to analyze the catalyst $Au/TiO_2$, to gain insight in the reaction and to develop an analysis method to quantify the reaction products. The concentration of diclofenac was first examined with a UV/VIS spectrophotometer at a wavelength of 276 nm. Next, when degradation was detected, HPLC was used to analyze the reaction products. After performing the reaction in batch, it was performed in the monolith.

The degradation of diclofenac is observed in the batch reactor with the UV/VIS spectrophotometer by an increase in absorbance, which was counterintuitive. Afterwards, the degradation was confirmed by the HPLC analysis. The concentration of diclofenac decreased, but the formed degradation products were absorbing at the same wavelength. So, a photocatalytic degradation of diclofenac took place.

# Abstract in Dutch

Het farmaceutische component diclofenac behandelt pijnen en ontstekingsreacties. Helaas metaboliseert het menselijk lichaam dit medicijn niet volledig waardoor het in het afvalwater belandt samen met zijn metabolieten. Na een traditionele afvalwaterzuiveringsbehandeling is diclofenac nog steeds aanwezig in het effluent in concentraties die de *Predicted No Effect Concentration* overschrijden. Het doel van deze masterscriptie was om diclofenac af te breken met behulp van fotochemie in een opschaalbare doorschijnende monolithische reactor. Deze reactor bestaat uit kleine, parallel naast elkaar geplaatste kanalen en werd gebruikt vanwege zijn hoge productiviteit en energie-efficiëntie.

Eerst werden experimenten uitgevoerd in batch reactoren om de katalysator $Au/TiO_2$ te analyseren, inzicht te krijgen in de reactie en een analysemethode te ontwikkelen om de reactieproducten te kwantificeren. De concentratie werd eerst gemeten met een UV/VIS-spectrofotometer bij een golflengte van 276 nm waarna een HPLC-analyse de reactieproducten analyseerde. Na het uitvoeren van de reactie in een batch reactor werd er overgeschakeld naar de monolithische reactor.

Fotokatalytische afbraak van diclofenac is waargenomen in de batch reactor. De UV/VIS-spectrofotometer meette eerst een verhoging in concentratie waarna de HPLC-analyse de degradatie bevestigde. De concentratie aan diclofenac verlaagde en afbraakproducten, die licht absorbeerden bij dezelfde golflengte, werden gevormd. Besloten is dat fotokatalytische degradatie van diclofenac plaatsvond.

# 1 Introduction

In the first part of this thesis the degradation of diclofenac in the first generation of translucent monoliths is discussed.

The research for this thesis takes place at CIPT. This is a research group that focuses on the intensification of chemical processes. CIPT develops new technologies for process intensification utilizing ultrasound, photochemistry and micro-flow reactors [1]. This thesis focuses on the development of a scalable micro-flow reactor to eliminate diclofenac (DCF) out of wastewater with photochemistry.

DCF is a pharmaceutical used to treat pain and inflammatory diseases effectively. Therefore 940 tons of DCF is consumed worldwide each year. The human body does not fully metabolize this medicine after administration. So, the non-metabolized parent medications and metabolites are excreted from the body by urine and feces and end up in the wastewater [2].

In consequence, DCF has to be eliminated by a wastewater treatment plant so that it is not harmful for the human body when taken in. A problem here is that, after a normal water treatment, consisting of: a primary purification, a biological cleaning and after-settlement, DCF is still in too high amounts detected in the wastewater [3]. So, a tertiary purification is necessary. A possible solution is a photocatalytic degradation to remove DCF.

Earlier was mentioned that the aim of this master's thesis is to try to eliminate DCF out of wastewater with the help of photochemistry. Photochemistry is a reaction that takes place under the influence of light [4]. Also, a catalyst is added which is responsible for changing the intrinsic mechanism of the reaction. A commonly used semiconductor heterogeneous catalyst is $TiO_2$ [5]. This process is termed a photocatalytic reaction.

The majority of photocatalytic reactions are performed in batch reactors, however this reactor has a major disadvantage. When it is irradiated with light, the light cannot reach the center of the reactor, hence the reaction slows down, lowering the reactors overall efficiency. The use of microreactors can be the solution for this disadvantage, because of their small channel. Light irradiates every single part of the channel so that every catalyst, also in the center, can be activated. Microreactors has also a large surface-to-volume ratio [5], [6].

During the experimental part of the thesis, first, preliminary experiments are performed in batch reactors. This to test the catalyst, to gain insight in the reaction and to develop an analysis method to quantify the reaction products. The moment the desired result is achieved, a switch is made to the microreactor.

After the photocatalytic reaction, the concentration of DCF is measured by several techniques to determine the conversion and reaction rate. The first detection technique is UV/VIS spectrophotometry, this is used to quantify the DCF concentration. When a decrease in DFC concentration is observed via this technique, there was switched to an advanced detection technique to determine the reaction production, high pressure liquid chromatography (HPLC). Another detection technique that can be used is the chemical oxygen demand (COD) to determine the amount of carbon inside the solution. If any volatile compounds are formed (e.g. $CO_2$), a decrease in COD is expected.

Last, another aim of this thesis is to optimize the degradation of DCF by varying the catalyst concentration, flow rate and light intensity.

In the second part of this project, an article discusses the validation of simulations of different monolith reactors.

As mentioned before, these days, photochemical reactions are performed in batch reactors, however these reactors have two major disadvantages: photon transfer limitations and mass transfer limitations.

These problems can be solved by the use of microreactors. This reactor consists of a small channel where the chemical reactions takes place. But this reactor has the disadvantage of a low overall energy efficiency. To solve this issue, a monolith reactor can be created consisting of small channels placed parallel next to each other. This 3D reactor captures the lost photons of the 2D reactor. This happens through the use of the set of channels placed behind the first set of channels. The energy efficiency and throughput increase.

The aim is to develop a monolith reactor with a high productivity and a high energy efficiency. To evaluate different reactors, the software program COMSOL is used. This program calculates ray tracing and computational fluid dynamics (CFD) of each channel. These parameters give information about the interaction between the light and the particle on the one hand and the throughput on the other. Out of these results, the space-time yield (STY) and the photochemical space-time yield (PSTY) can be calculated. These parameters give information about the productivity and the amount of product produced by a volumetric specific yield per power and unit of time which makes it possible to compare the different designs.

# 2 Literature review

## 2.1 Wastewater

Every day, every single person consumes 120 L domestic wastewater. Today, a treatment plant can already clean 84 % of all this domestic wastewater [3].

The wastewater is composed of domestic wastewater, wastewater from hospitals and wastewater from industrial sites. This water contains a lot of different components, herbicides, pesticide, and inorganic compounds (such as heavy metals, mercury, cadmium, lead, etc.). Medication and numerous pathogenic micro-organisms are also found in wastewater which has genotoxic, mutagenic and carcinogenic effects. Furthermore, nutrients are also traced in the wastewater, some of these nutrients stimulate the growth of plants, others may be toxic [7], [8].

Besides the wastewater, some drugs such as DCF are still present in the effluent. The concentration of some medications is too high in the effluent which has a harmful effect on the human body, animals and nature. The factors responsible for tracing the drugs in wastewater are the amount of people who takes the drugs, the frequency of intake, the doses of intake and the excretion factor [7].

## 2.2 Diclofenac in wastewater

DCF, 2-[2-(2,6-dichloroanilino)phenyl]acetic acid, is one of the most present components in wastewater. Each year, about 940 tons of DCF is consumed worldwide. DCF is a non-steroidal anti-inflammatory drug and also used as painkiller. It can be taken orally, dermally, rectally and intramuscularly. The molecular formula, $C_{14}H_{11}C_{12}NO_2$, of this drug is shown in Figure 1 [2].

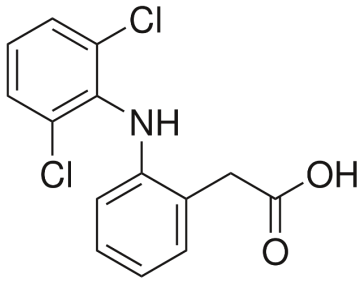


Figure 1: The molecular formula of DCF [2, p.1152]

Some medicines are not fully metabolized after administration. Non-metabolized parent medications are excreted from the body by urine and feces. The allowable amount for taking DCF is 75–150 mg daily. After oral intake of DCF, the drug is halved after two hours. 65 percent of the medication and metabolites leave the human body and end up in the wastewater. The metabolites of DCF are 5'-OH-DFC, 4'-OH-DFC, 3'-OH-DFC, 4'-5-diOH-DFC, 4'-OH-5-Cl- DFC, 3'-OH-DCF. These are hydroxylated metabolites. Further a methoxylated derivative, 3'-OH-4'-$CH_3$O-DFC, is also metabolized [2], [9].

Various studies indicate that the intake of contaminated wastewater with DCF disrupts biochemical functions and damages tissues, liver and kidney cell function of aquatic animals [9]. DCF is a drug detected in the effluent with a concentration of 503 ng/L. This concentration is above the minimal and maximal Predicted No Effect Concentration (PNEC). The minimal PNEC for DCF is 100 ng/L as is the maximal PNEC [7].

Table 1 gives information about the physicals and chemicals of DCF.

Table 1: Physical and chemical information about DCF [2], [9]

| | MM ($g\ mol^{-1}$) | Vapor pressure (mm Hg) | pKa (20 °C) | Log $K_{ow}$ | H (at $m^3\ m^{-1}$) | Solubility ($mg\ L^{-1}$) |
|---|---|---|---|---|---|---|
| Diclofenac | 292.2 | $6.14 \times 10^{-8}$ | 4.1 – 4.5 | 1.9 – 4.5 | $4.7 \times 10^{-12}$ | 2.37 |

## 2.3 Wastewater treatment

In the treatment plant, wastewater is collected in a collection point and is controlled by a fine sieve. Big waste is stopped by the sieves and the filtered water undergoes a primary purification.

The primary purification contains fine filters to remove particles in solution. At some installations, the wastewater is brought through a grease- and sand trap. The grease trap is used to remove fats and oils. The sand trap ensures that the sand and gravel settle down. This step is the mechanical pre-treatment.

In the secondary step, micro-organisms are used. This step is called the biological cleaning. These organisms, also known as activated sludge, use the waste in the water as food, which keeps them alive and makes them grow. During this step, an aeration basin bubbles oxygen through the water, so the organisms are able to survive in this water. The oxygen helps to break down the carbon compounds in the water to carbon dioxide and water. The water also contains phosphor and nitrogen which can be removed by switching the aeration on and off.

A last step is required to settle down the sludge to the bottom. At the end of this process, the sludge is collected in a central well. A substantial part of the sludge is returned to the start of the biological cleaning and the cycle can start again [3], [7].

Now, the water is completely purified by the capacity of the water treatment plant. However, some components, like DCF, are not fully biodegradable and have not yet been completely removed out of the water. So, a tertiary treatment is necessary. A lot of techniques can be used to remove these non-biodegradable components such as adsorption with active carbon, coagulation and flocculation, oxidation, reduction and stripping [7], [10].

## 2.4 Degradation reaction capabilities

To trigger a chemical reaction, the activation energy must be reached. This can be realized by adding external energy. For example, one of the most usable techniques is to add chemical reagents. These reagents are used for the degradation of these non-biodegradable components, into the water. This process happens under high temperature and pressure, and with the addition of expensive and/or toxic catalysts. This technique is applied in a batch reactor, takes a lot of time and is energy intensive. Furthermore, specialized equipment is needed to guarantee the process safety at these high temperatures and pressures [11].

Instead of utilizing a process under high temperature and pressure, light can be used to supply the activation energy. A distinction can be made between two forms of photochemical reactions: direct photolysis and advanced oxidation processes (AOP) [4]. In the first case, the waste in the water directly absorbs the light which lead to degradation [4]. In the second case, a photocatalyst absorbs the light and forms reactive oxygen species (ROS). These species oxidize the organic material [4]. There are several processes to create these ROS, such as ozone/hydroxide ion ($O_3/OH^-$), ozone/hydrogen peroxide ($O_3/H_2O_2$), ozone/ultraviolet radiation ($O_3$/UV), hydrogen peroxide/UV radiation ($UV/H_2O_2$), ozone/heterogeneous catalysts (HCO), photo Fenton ($UV/H_2O_2/Fe^{2+}$) and heterogeneous photocatalysis ($UV/TiO_2$). These types of AOP's increase the oxidation power. As mentioned, this is done by forming

reactive OH radicals from an oxidant and a catalyst which has a higher oxidation power than the oxidants normally used [6], [10].

The catalyst is responsible for changing the intrinsic mechanism of the reaction which leads to a decrease of the activation energy. Subsequently, water-polluting substances are converted by these radicals into carbon dioxide, water and stable mineral acids [6], [12].

This technique makes it possible to reduce the number of chemical reagents and improve the efficiency of water treatment processes. A disadvantage of the use of photocatalysis in a batch reactor is the fact that the light is not able to penetrate through this reactor to the center if a high catalyst concentration is used [5].

Nevertheless, the batch reactor can be replaced by a more efficient reactor, a microreactor. In a microreactor, the chemical reaction takes place in a small channel, so the light irradiates the entire channel even when utilizing a high catalyst concentration. Furthermore, the aforementioned security issues are solved. For example, an explosion of a batch reactor can have big consequences, which includes financial losses and injuries. However, an explosion in a microreactor has fewer consequences. Also, the process in a microreactor is no longer as time-consuming as the process in a batch reactor [5].

All of these topics will be discussed in detail in the following sections.

## 2.5 Photochemistry

Photochemistry is a technique that takes place under the influence of light which makes a reaction possible by absorbing photons. This technique does not use any source of heat to get an electron in excited state. With photochemistry, reactions pathways are accessible that are otherwise impossible for conventional thermochemical reactions [4]. Some advantages of photochemistry are the increase in selectivity, the mild reaction conditions and low demand for organic solvents. Nevertheless, photochemistry has some drawbacks. One of them is their low reaction rate. Another one is their low energy efficiency [13].

To begin, light is a bundle of photons which carry the energy of light. When light is absorbed by the target molecule, the photon gives its energy to this molecule. The process ensures some changes in the electrical structure of the molecule which makes it possible to react in a different way. The molecule is now in an excited state.

To explain how it is possible for a molecule to switch to an excited state, the atomic structure and electromagnetic radiation has to be discussed.

### 2.5.1 Atomic structure

An atom consists of an atomic nucleus, with protons, neutrons and some electronic shells around the nucleus. The number of protons and electrons is the same in an atom which leads to a neutral atom. The main quantum number (n) gives the number of electronic shells per atom. The shell the closest to the atomic nucleus has the smallest radius and the lowest energy. The radius of a shell increases with the number of shells. Also, the energy increases when the number of shells increases. Each shell can count a maximum of electrons, $2\ n^2$. The atomic number of an element gives the number of electrons and consequently the number of electronic shells. The electrons on the outer shell are called the valence electrons [14].

Furthermore, an electron has a dual character. This means, it has a particle- and a wave character. Schrödinger described the electron as a mathematical wave function ($\psi$). The square of the wave function ($\psi^2$) provides information about the position of the electron. This is called the orbital. As mentioned before, the main quantum number gives information about the energy level of the electron

and the distance to the nucleus. The energy levels are divided into sublevels. The azimuthal quantum number (l) gives information about the shape of the orbital. Orbitals on the same sublevel have the same energy. The magnetic quantum number (m) tells something about the orientation of the orbital. Each electron in an atom with multiple electrons is attracted by the nucleus and is repelled by the other electrons. An electron on the outer shell can be shielded from the nucleus by the electrons in between [14].

Later studies showed that an electron has an intrinsic property, the electronic spin. An electron spins around his own axis. It can have a spin-up (↑) or a spin-down (↓). A spinning electron is a moving electrical charge and induces a magnetic field. Two spinning electrons with an opposite spin in the same orbital are called a singlet. This level is the quaternal quantum number [14].

Next, the state of an electron can be described by the four quantum numbers, but Pauli's exclusion principle tells that two electrons never have the same conditions over all four quantum numbers [14].

Last, the electronic configuration gives information about the electrons in the different levels and orbitals divided in the atom. The ground state is the state with the lowest energy level. This level is achieved when orbitals on the same level contain as much as possible electrons with the same spin [14].

### 2.5.2 Electromagnetic radiation

Light is necessary to start a photochemical reaction. Visible (VIS)- (380 nm - 780 nm) and ultraviolet (UV)-radiation (10 nm – 400 nm) are a kind of electromagnetic radiation. Electromagnetic radiation is the reproduction of electric and magnetic oscillations through space. Radiation is described as a double wave. The maximum amplitude of the electric wave (E) and the magnetic field (H) are perpendicular to each other. The wave moves perpendicularly to both directions with a certain propagation speed that is dependent on the nature of the medium. The smallest distance between two places with the same electromagnetic conditions is called the wavelength (λ). The number of wavelengths which an electromagnetic wave follows per second is called the frequency (f). The wavelength and the frequency are inversely proportional to each other. As mentioned before, electromagnetic waves are a stream of photons. The number of photons observed per unit time is called the photon flux and has affect the intrinsic reaction rate of photochemical processes [15]. Figure 2 presents all the mentioned terms.

The relation between the energy of a photon and its wavelength is described by equation (1).

$$E = h\ f \tag{1}$$

$E$ = The energy of the photons of light (J)
$h$ = The Planck's constant ($6.63 \times 10^{-34}$ J s)
$f$ = The frequency (Hz)

Equation (2) gives the relation between wavelength and frequency.

$$c = \lambda\ f \tag{2}$$

$c$ = The speed of the wave ($c_{Light} \approx 3.00 \times 10^{8}$ m $s^{-1}$)
$\lambda$ = The wavelength (m)
$f$ = The frequency (Hz)

These two formulas can be combined with each other to equation (3) [16].

$$E = h\ \frac{c}{\lambda} \tag{3}$$

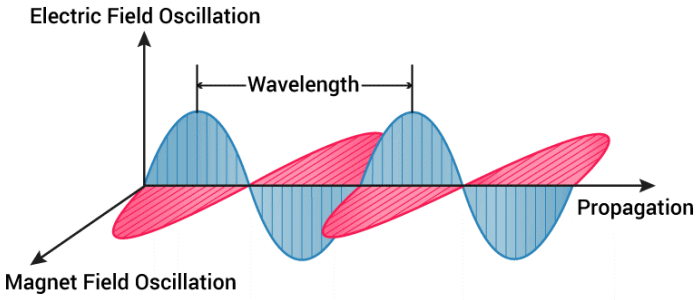


Figure 2: Illustration of the propagation of electromagnetic radiation [17]

### 2.5.3 Photochemical reaction

It is necessary that three fundamental principles take place in order for photochemistry to happen:

1. the first law, the Grotthuss-Draper law, states that it is essential that the target molecule must absorb the light to make it possible for a photochemical reaction to happen. It is perfectly possible to expose the molecules to light without absorbing energy [10].

   The probability that the light absorption takes place, is indicated by the molar absorption coefficient and is a measurement of the probability that the interaction of a molecule results in light absorption. This results in excitation of the molecule. This parameter can be found in Lambert-Beer's law, equation (4). This law says that the absorbance is directly proportional to the concentration of the light-absorbing compound [10], [18];

   $$E = \varepsilon \; c \; d \tag{4}$$

   $E$ = The absorbance
   $\varepsilon$ = The molar extinction coefficient (l $\text{mol}^{-1}$ $\text{cm}^{-1}$)
   $c$ = The concentration of light-absorbing compound (mol $\text{l}^{-1}$)
   $d$ = The path length (cm)

2. the second law, the Stark-Einstein law, states that each molecule absorbs one photon and is activated by this photon [19];

3. the third law, the Bunson-Roscoe law, states that the amount of product, of a photochemical reaction, is directly proportional to the total energy dose. The total energy dose depends on both the radiation intensity and the exposure time independent of the type of source [10].

Also, there are some influencing factors which have to be noted. Firstly, the presence of suspended solids and interfering substances are an important factor. These suspended solids can scatter the light or can absorb the light which leads to the reduction of the radiation intensity. Secondly, substances that give rise to deposits on the lamp must be avoided. This disposition causes a decrease of the light intensity that reaches the organic material. The efficiency of the reaction decreases. In this case, the lamp is not in contact with the water so, the hardness of the water or other substances do not influence the radiation intensity by depositing the lamp [10].

One of the biggest advantages of photochemistry is the selectivity. A specific wavelength band can make a specific bond type go in excited state. As mentioned, there is a whole spectrum of wavelengths that can be used to make different types of bond types go in excited state which leads to a high selectivity [4].

Once the molecule has absorbed the light energy, it changes from ground state to excited state. There are several possibilities what the molecule can do next. One option is that the molecule in an excited state, emits the absorbed light and goes back to the ground state. This process is called fluorescence.

The energy can also be released in the form of light in an intersystem, phosphorescence. The excited singlet state is crossed to a triplet state. The difference between triplet state and the singlet is the spin of the excited electron [20]. The difference between these two mechanisms is shown in Figure 3.

Another option is that the molecule goes back to the ground state by losing the energy in the form of heat, internal conversion. A fourth option is that the molecule can use the energy to fall apart, to rearrange the molecule, isomerize, dimerize, eliminate or add small molecules. The energy can also be used to transfer to another molecule [14].

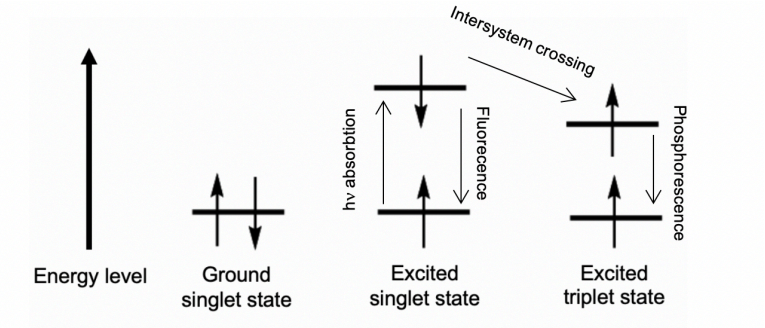


Figure 3: Illustration of the principles of fluorescence and phosphorescence [20]

## 2.6 Light sources

The most common light sources used for a photochemical reaction are UV-lamps (mercury lamps), Xenon lamps and light-emitting diode (LED). UV-light falls just outside the spectrum of VIS-light. It has a shorter wavelength than VIS-light, so UV-light contains a higher energy. [15], [21].

LED is a diode that consists of an electronic semiconductor component. When current passes through, electromagnetic radiation is emitted in the form of UV, VIS or heat. The power of this radiation is called optical power and can be calculated with equation (5).

$$P = U\ I\ \kappa \tag{5}$$

$P$ = Optical power (Watt)
$U$ = Source voltage (volt)
The labour required to transport a positive unit load from the negative clamp to the positive clamp via the source. The labour is supplied by the source.
$I$ = Current (ampere)
The amount of charge passing through any cross-section of a conductor per unit time.
$\kappa$ = Efficiency factor of the lamp

Normally, the efficiency of a LED-lamp is over 10 % and mostly is in between 40 and 50 % [22], [23]. Furthermore, it has a lot of advantages, such as a long lifetime and a fast response time (µs). Its power and environmental protection are two other advantages. At last, it has a good mechanical property which means that LED is resistance to mechanical disturbances like shocks and impacts [4], [24].

## 2.7 Photocatalyst

As mentioned, a catalyst is responsible for changing the intrinsic mechanism of the reaction which leads to a decrease of the activation energy. A photocatalyst is activated by light from a certain frequency and catalyzes a reaction. The catalyst releases electrons, as a result of irradiation, to the target molecule to oxidize it to $H_2O$, $CO_2$ and stable mineral acids [4], [12].

There are two types of catalysts: a heterogeneous catalyst and a homogeneous catalyst. The difference between those types is the phase of the catalyst. On the one hand, a homogeneous catalyst is in the same phase as the reagent. An advantage of this catalyst is that it makes optimal contact with the reagent so mass transfer is not a problem. A disadvantage of this type is that after the process, an additional purification step is necessary. On the other hand, a heterogeneous catalyst is in a different phase than the reagent. A purification step is not always applicable in this process. When the catalyst is immobilized to the walls of the reactor, a purification step is not applicable. But a heterogeneous catalyst can also be brought in suspension. So, in this case a purification step is still necessary. Another disadvantage of this catalyst is that the mass transfer is not as good as with a homogeneous catalyst [6], [25].

### 2.7.1 Titanium dioxide photocatalysis

A commonly used semiconductor heterogeneous catalyst is $TiO_2$. $TiO_2$ is a non-toxic and safe catalyst with a high photosensitivity and is very stable. It is one of the most active photocatalyst and owns an energy band gap of 3.2 eV. A band gap is the energy difference between the bottom of the conductor band and the top of the valence band of semiconductors [26], [27].

In this case, it means that the catalyst has to be irradiated with light with a wavelength around 380 nm or less to make electrons go in an excited state. So, UV-light, can be optimally absorbed with this catalyst. Only 5 % of the solar light exist of UV-light, which means that it is necessary to make sure the catalyst changes in excited state with light with a lower energy level.

This can be realized by doping $TiO_2$ with metallic nanoparticles, with gold as one of the most interesting particles. An important advantage of the metal nanoparticle is that it is possible to let the electron go in excited state by irradiation of VIS-light. This light has a lower energy level than UV-light which means a higher golf length. Au/$TiO_2$ absorbs light with a golf length from 430 to 700 nm. Another advantage of the nanoparticles is that these elements make sure the electron does not fall down to the valence shell [26], [27].

### 2.7.2 The photocatalytic reaction mechanism

The formation of an electron-hole pair is the result of this photoexcitation. This means, the catalyst lost one electron and the remaining element is loaded positive. The excited electron is used in a reduction reaction with dissolved oxygen to create a superoxide radical ($O_2^{\bullet -}$). It is very important that there is enough dissolved oxygen in the wastewater to make this radical and to prevent an electron-hole recombination. The electron-hole causes an oxidation reaction with the absorbed water which forms $OH^{\bullet}$. The superoxide radical can react with $OH^{\bullet}$ to a hydroperoxyl radical ($HOO^{\bullet}$) which can react further to $H_2O_2$ [5]. $H_2O_2$ can then participate in the degradation pathway by functioning as an electron acceptor or by disintegrating into OH radicals through homolytic cleavage [4]. These reactions take place at the surface of the catalyst and there can be deduced that it is necessary that this process has to be carried out in the presence of water and sufficiently dissolved oxygen [5]. The reaction mechanism is illustrated in Figure 4.

Photoexcitation: $TiO_2 \rightarrow e^- + h^+$
Reduction: $O_2 + e^- \rightarrow O_2^{\bullet -}$
Oxidation: $OH^- + h^+ \rightarrow OH^{\bullet}$

The formation of $H_2O_2$ out of $O_2^{\bullet -}$ and $OH^{\bullet}$:
$O_2^{\bullet -} + OH^{\bullet} \rightarrow HOO^{\bullet}$
$HOO^{\bullet} + e^- \rightarrow HO_2^-$
$HO_2^- + H^+ \rightarrow H_2O_2$

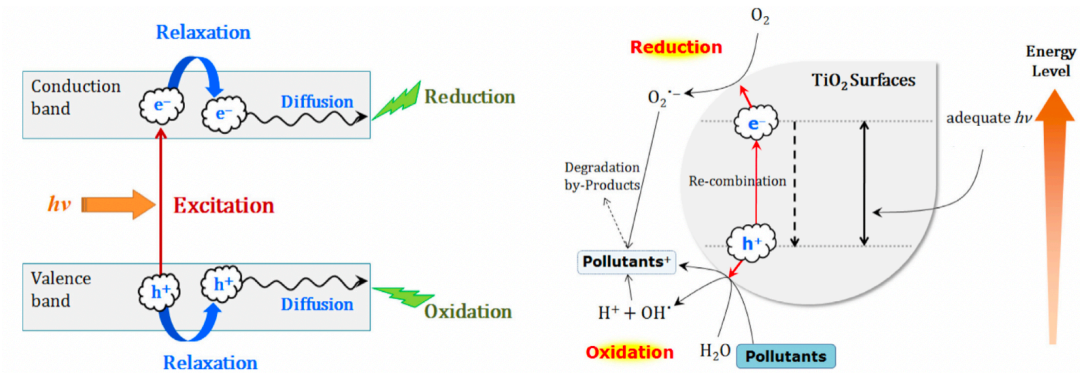


Figure 4: Schematic visualization of the formation of an electron-hole pair [28, p. 1764]

The mechanism of the photocatalytic process consists out of several steps and is shown in Figure 5. The first step is the mass transfer of the medical product from the bulk to the surface of the $TiO_2$ catalyst. In this case, diffusion takes place because the product has to go from a liquid phase, wastewater, to a solid phase, the photocatalyst. The second step is the absorption of the medical product to the activated surface of the $TiO_2$ nanoparticle. The photocatalytic reaction, desorption of the products and diffusion from the surface of the photo catalyst to the bulk are the following steps [5].

Mass transfer is a very important step in this process because of the waste has to reach the surface of the catalyst to react. Nevertheless, there are some rate limiting steps among which film diffusion. This can be solved by mixing faster. The film becomes smaller, so the diffusion distance is shorter [12].

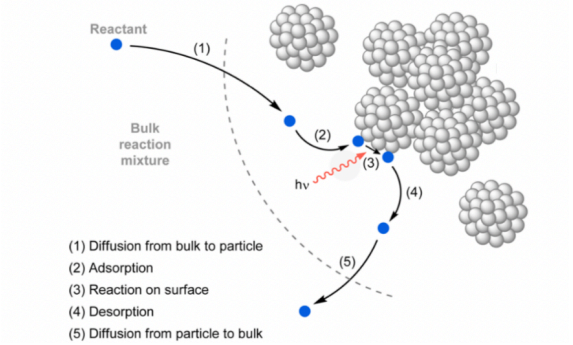


Figure 5: An illustration of the mechanism of the photocatalytic process [5, p. 10323]

### 2.7.3 Influencing parameters

The absorption to the catalyst surface can be influenced by the pH. This has namely an effect on the surface charge of the photocatalyst. The isoelectric point of $TiO_2$ is around 6.25. Due to a pH lower than 6.25, the surface becomes positive and vice versa. As mentioned before, the isoelectric point of DCF is around 4.3 and is not soluble below a pH of 4.00. So, the optimal pH for the best absorption lies around 6.00 [21].

Also, the temperature plays a role in the operation of the catalyst. 80 °C is a limit temperature. By dropping the temperature, the surface absorption increases which is an advantage. However, when the temperature rises, the electron-hole recombination increases, which has a negative effect on the degradation rate.

Another limitation factor is the concentration. At the moment that the catalyst is saturated due to an excessive amount of pollutant, the surplus pollutant is no longer broken down. Too many pollutants can also scatter the light, so the catalyst is not activated. Also, the concentration of catalyst is an important factor. More catalyst leads to more surface area which leads to more degradation. But too much catalyst also scatters the light, so HO radicals can't be formed and the degradation slows down [4], [21].

At last, the light distribution can also lead to limitations. Irradiation of the catalyst forms electron-hole pairs which makes a reaction possible. So, the reaction rate is proportional to the irradiation distribution. When the intensity of the light increases, more electron-hole pairs are formed. Not every electron-hole pair leads to a reaction because the concentration of the organic material is too low. Some electron-hole pairs recombine and make a reaction no longer possible, lowering the photonic efficiency [4].

## 2.8 Degradation products of diclofenac

When a photocatalytic reaction takes place on DCF, some degradation products are formed. DCF falls apart into eight reaction products.

A first pathway during the degradation of DCF is the loss of chlorine and hydrogen atoms. Next, a new ring is formed as a result of a structural rearrangement. 2-(8-chloro-9H-carbazol-1-yl) acetic acid (1) is formed. In this intermediary the chlorine is replaced by a $HO^-$. The result of this substitution is genesis of 2-(8-hydroxy-9H-carbazol-1-yl) acetic acid (3). From 1, also 1-chloro-8-methyl-9H-carbazole (2) can be formed as a result of a decarboxylation. This intermediary can also lose its chlorine. But in this case, a hydrogen addition takes place. The intermediary 1-methyl-9H-carbazole (4) is formed. 2 can also undergo a HO-radical addition which leads to genesis of 8-chloro-9H-carbazole-1-carboxylic acid (5).

In another pathway, DCF undergoes a decarboxylation. The intermediary 2,6-dichloro-N-o-tolylbenzenamine (6) is formed. On this intermediary a HO-radical addition can take place which leads to the formation of 2-(2,6-dichlorophenylamino)phenyl)methanol (7). Next, this intermediary can lose its chlorines and an oxidation can take place. The intermediary 2-(phenylamino)benzaldehyde (8) is formed [21], [29], [30], [31], [32]. This reaction mechanism is shown in Figure 6.

During this process, a pH decrease takes place. This as result of the formation of the degradation products and release of HCl and $CO_2$ [21].

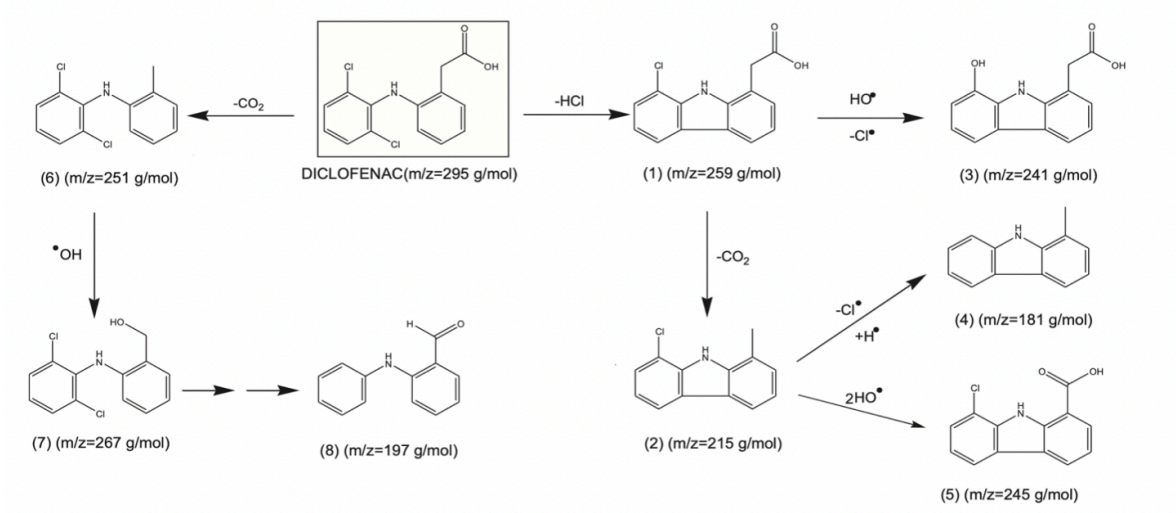


Figure 6: A schematical presentation about the reaction mechanism of the degradation of DCF [30, p. 116]

## 2.9 Reactor design

The geometry of a reactor is of uttermost importance to the productivity since it influences the reaction rate. As already mentioned, two mains issues of the current design of reactors are mass and photon transfer limitations. These problems will be discussed in the upcoming section.

### 2.9.1 Batch reactor

A batch reactor is a reactor consisting of a vessel containing all the reagents that are required to perform the desired reaction. The reactor is brought into the right conditions and is mixed during the entire process. This process runs for a certain amount of time and the reactor is completely emptied at the end.

A major disadvantage is that when it is irradiated with light, the light cannot reach the center of the reactor, so the reaction slows down in these dark areas [5].

The reaction time is the time how long the reagents remain in the reactor. Longer reaction times are obtained because the mass transfer, from one phase to the other, takes place slowly in a batch reactor. This is possible because the interfacial area is low and poorly defined. As mentioned before, the mass transfer limitation can be solved by mixing faster so the film becomes smaller and the diffusion distance shorter [5], [12].

Because of the whole reaction mixture is in the reactor, during the entire process, unwanted subsequent reactions or dissolution take place [33].

### 2.9.2 Microreactor

Microreactors are very small reactors, which have a channel inside where the chemical reactions take place. Microreactors are conducted in flow as opposed to batch reactors. This means, the reagents are pumped through the channel [5]. So, a first disadvantage of the batch reactor is solved. By pumping the mixture through the reactor, the mixture is removed after it has passed the whole reactor. Unwanted subsequent reactions or dissolution are reduced or shut down [33].

Furthermore, the design of the microreactor is very important for the reactions to take place under optimal conditions. It is necessary that the channel is transparent so the light can go through and prevent dark areas. An advantage of this small channel is that the light hits every single part of the channel so that every catalyst, also in the center, can be activated [5].

Another advantage of the microreactor is the large surface-to-volume ratio, which ensures improved photon transport phenomena and improved mass and heat transfer. It also ensures efficient heat dissipation. This is important to keep the reaction temperature stable so that no unwanted by-products can be formed via thermal paths. Microreactors are therefore called isothermal reactors. The surface characteristics and material properties also play an important role in the heat management of the reactor. Strong heat-conducting material is able to release heat more easily, so that the reaction temperature can be kept stable more easily than poor heat-conducting material [5]. The pressure and residence time are also under effective control which makes a microreactor safer than a batch reactor [33].

For a microreactor, the reaction time is the average time that the reactants spend in the reactor. These reactors have an internal diameter of less than or equal to 1 mm. Laminar flow takes place in these channels. This means that the liquid flows over each other in parallel layers, as shown in Figure 7. Mixing takes place by diffusion from one layer to the other. The smaller the diameter of a channel, the faster uniform distribution over the channel is achieved. It is important that the mixing time must always be shorter than the reaction time so that the desired reactions can take place. It is also of great value that good flow channeling takes place in order to reduce death volume/stationary volume, thereby reducing the volume of the reactor [5], [34], [35].

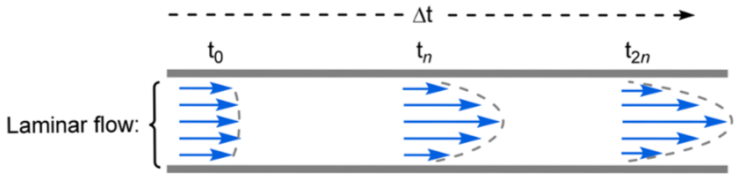


Figure 7: Illustration of the laminar flow in a microreactor [5, p. 10279]

To scale up a microreactor, two methods can be applied.

The first way is to increase the flow rates, thereby an increase of throughput. An advantage of this technique is that the reaction times can be shortened because a higher mass and heat transfer takes place. A disadvantage of this method is that the energy dissipation across the reactor increases as a result of the pressure drop [5].

The second technique is numbering-up. Here, several microreactors are placed parallel to each other. A distinction is made between two types of numbering-up. In the first method, several microreactors are placed in parallel with their process control and pump system, which has the advantage if at the moment one reactor fails, it has no influence on the other reactors. A disadvantage is the fact that this method is very expensive. This way is called external numbering-up. The second method, internal numbering-up, is cheaper. Here, the reactor itself is numbering-up and the process control and the pumping system are distributed over the reactor. The distributor section is an essential part of this method since uneven reaction conditions are the result of small differences in pressure drop [5].

### 2.9.3 Monolith reactor

A major disadvantage of the microreactors is the low overall energy efficiency. This is caused by the photons that cannot transfer their energy to the catalyst because the majority of them do not end up in the reaction channel. To solve this problem, a 3D microreactor can be developed. The lost photons of the 2D reactor are captured by the set of channels placed behind the first set of channels. The energy efficiency and throughput increase. This reactor is called a monolith [13]. This phenomenon is shown in Figure 8.

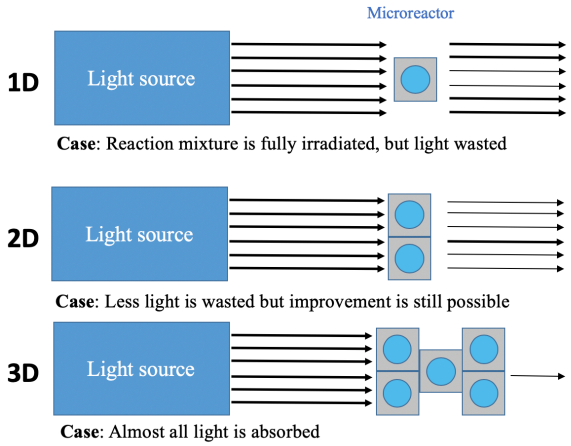


Figure 8: Illustration about the disadvantage of 1D and 2D microreactors in contrast with a 3D microreactor [36]

The several reactor types are illustrated in Figure 9.

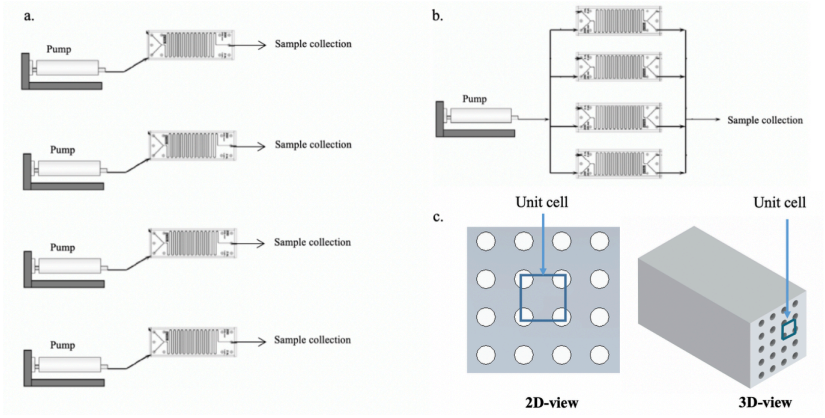


Figure 9: a. A visualization of external numbering-up [37, p. 141]; b. An illustration of internal numbering-up [37, p. 141]; c. A schematic presentation of a monolith reactor [36]

## 2.10 Material

### 2.10.1 3D-printer

In this research a monolith reactor is printed with a 3D-printer. There are two principles commonly used to print an object.

The first principle is fused deposition modeling (FDM). This is a technique where the object is built by editing layer by layer. The material is melted and is brought on the next layer. By moving the nozzle of the printer, the right pattern is created [38].

A second principle is stereolithography apparatus (SLA). This technique uses a UV-laser to cure the resin in the right pattern. It means, the resin is liquid at the beginning of the printing. SLA works also layer by layer. Because of the accuracy of SLA, this technique is used to print the monolith [39].

### 2.10.2 UV/VIS spectrophotometry

The UV/VIS spectrophotometry is a quantity analysis technique to measure the concentration of a chemical compound. The concentration of DCF, in this case, is determined by how much light is absorbed by the chemical compounds and the number of photons that passes through the sample. Every chemical product absorbs light with a specific wavelength. So, it is important to first measure the absorption spectrum of the compounds to determine its maximum absorption. The possible spectrum to measure this absorption in, is in the UV- and VIS-spectrum, between 190 and 1100 nm.

A spectrophotometer consists of two parts. The spectrometer is the first part. This sends out light with a specific wavelength. The monochromator receives a straight bundle of light coming from the collimator. The monochromator splits the light in a spectrum. Next, the sample absorbs a specific wavelength. After this, the photometer sends a signal to the galvanometer or a digital display based on the amount of light passed through the sample. This principle is shown in Figure 10. In conclusion, the concentration of the chemical compound can be measured by Lambert-Beer's law, equation (4) [18], [40].

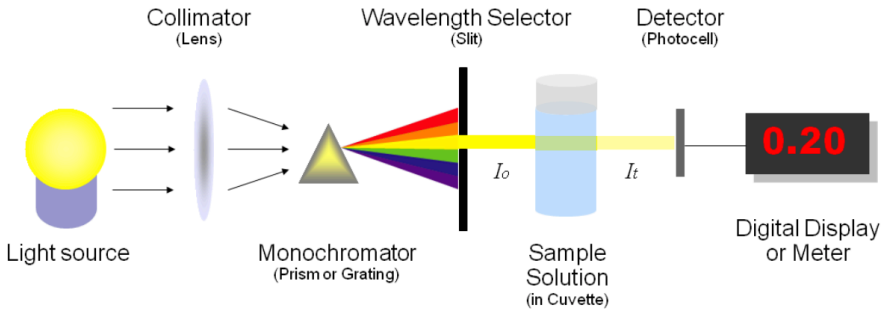


Figure 10: A presentation of the principle of a UV/VIS spectrophotometer [40]

### 2.10.3 High pressure liquid chromatography

HPLC is a separation technique that separates compounds in a liquid phase by pumping it, under high pressure, through a packed column.

There is a difference between normal phase chromatography and reversed phase chromatography. When a polar stationary phase and a non-polar mobile phase are used, the phenomenon normal phase chromatography arises. In this case, polar molecules absorb strongly to the stationary phase. The non-polar molecules are taken with by the mobile phase. Later, the least polar molecules are deleted from the column by the non-polar mobile phase. The time that a compound needs to leave the column is defined as the retention time. The separation is based on a difference in hydrophobicity between the different compounds. The technique used, is based on reversible absorption and desorption. Reversed phase chromatography is the opposite.

A C18 column is one of the most commonly used columns. In this case, reversed phase chromatography is maintained. The column contains a non-polar stationary phase composed of silica particles with linear C18 carbon compounds.

Within the mobile phase, a distinction can be made between isocratic chromatography and gradient chromatography. Isocratic chromatography utilizes a mobile phase with constantly the same composition. When the percentages of the mobile phase increase during the run, gradient chromatography is applied.

A HPLC instrument consist of three sections: a pump, a UV-monitor and a processor. The pump is responsible for pumping samples through the column. When the injector is connected to the system, the injector takes up a solution and the solution is brought through the column. Next, the absorption of the compounds, which has left the column, are measured by a specific wavelength of the UV-monitor. This information is sent to the processor and this section prints a chromatogram. The chromatogram shows the order, linked to the retention time, of the different compounds. As mentioned, the retention time is depending on the polarity of the products. The area under the curve gives information about the concentration of each compound [41].

The principle of this technique is illustrated in Figure 11.

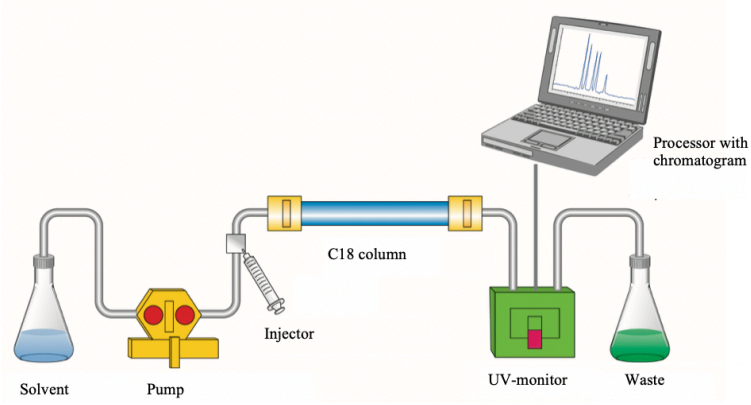


Figure 11: An illustration of the principle of HPLC [42]

### 2.10.4 Chemical oxygen demand

COD is a third technique to determine the carbon concentration. This is a technique where dichromate is used to oxidize the organic materials under acidic conditions. During the oxidation, oxygen is used to continue the process and leads to the production of $Cr^{3+}$. The amount of the remaining $Cr^{6+}$ or the produced $Cr^{3+}$ can be measured with a colorimetric determination technique and give information about the initial concentration of the organic materials [43].

# 3 Material and Method

## 3.1 Material

For the experiments, diclofenac sodium salt was supplied by VWR. This product has a purification of more than 98 %. The catalyst used in this research is the $Au/TiO_2$ catalyst delivered by Strem chemicals. The catalyst consists of 1 % gold and 98 % $TiO_2$. Further, in this experiment a comparison is made between the spectra of $TiO_2$ and $Au/TiO_2$. The catalyst $TiO_2$ was purchased from VWR and has a purity of > 99.5 %. When the reaction mixture is made, ultrapure water is used, purified by a device supplied by Sartorius.

When the reaction mixture is ready, the reaction can start. For the radiation, a CREE HighPower LED is used. This lamp was purchased from Conrad and has a maximal capacity of 40 W and a radiation angle of 115 °. In a first experiment, the Basetech BT-305 is used as a power source. This source was also supplied by Conrad. The voltage can be regulated between 0 and 30 V. The current is also adjustable. This from 0 to 5 A. So, the maximum power that can be supplied by this source is 150 W. In a second test setup, two constant current LED-drivers are used, produced by Barthelme. The maximal voltage is equal to 32 V and the current is adjustable with a setting screw till a maximum of 1000 mA.

Once the reaction takes place, the degradation has to be measured. First, a Genesys 10S UV/VIS spectrophotometer detects the concentration of the compounds. The spectrometer was purchased from ThermoFisher. Next, the degradation and the production of reaction products are measured with a HPLC device supplied by Agilent. As stationary phase, an Agilent Eclipse XDB-C18 column is applied (2.1 x 150 mm; 3.5 µm). A third way of measuring concentration is by means of COD. The Macherey-Nagel Nanocolor COD 1500 purchased from Fisher scientific is used. To heat the cuvettes, the Macherey-Nagel heating block is purchased and to measure the oxygen concentration, the Macherey-Nagel photometer is acquired.

When switched to the monolith reactor, the reactor is printed with the 3D-printer Form 2 purchased from Formlabs. It has a resolution of 100 µm. The resin used in this case is the Clear resin v4. The mixture is pumped through the monolith reactor by the use of the diaphragm liquid transfer pump, Liquiport NF 100, supplied by KNF.

## 3.2 Method

This thesis consists of 3 parts: a startup reaction in a batch reactor, the actual reaction in the monolith reaction and the optimization of degradation reaction.

### 3.2.1 Setup batch reactor

As mentioned before, the first experiments are performed in batch reactors to test the catalyst, to gain insight in the reaction and to develop an analysis method. Three reactors are set up. The first reactor contains DCF, the photocatalyst and light. The second reactor contains only DCF and light and the last reactor contains DCF and the photocatalyst but is performed in the dark. This set up is shown in Figure 12. The solution is measured after several hours and filtrated with a 0.45 µm filter to remove the catalyst.

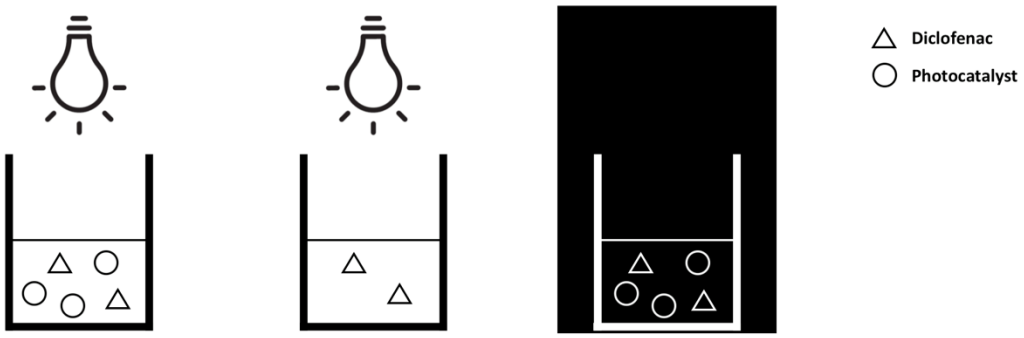


Figure 12: A schematic presentation of the preliminary experiments performed in batch reactors

A typical experiment consists of 0.1 mM DCF and 0.1 g/L Au/$TiO_2$. A beaker of 400 mL is used as a reactor. The total reaction volume is equal to 100 mL and consists of the needed compounds into ultrapure water. The diameter of the reactor is equal to 8 cm and the height is 11.5 cm. The reactor is placed onto a stirring plate and mixed with 300 rpm. On top of the reactor, the LED-lamp is placed, first connected to the Basetech BT-305 power source and later to two constant current LED-drivers. The temperature of the lamp is measured constantly by a thermometer because overheating can damage the lamp. This is caused by the large amount of energy that the lamp releases in the form of heat instead of light. The setup is cooled constantly to control this temperature. The setup is shown in Figure 13.


Figure 13: Setup batch reactor (the power source is not shown in this figure)

This experiment took several weeks. During these weeks several setups were tested. The first setup consisted of the LED-lamp connected to the Basetech BT-305. The distance between the surface of the mixture and the lamp was 25 cm. The voltage across the lamp was 32.1 V and the current flowing through the lamp was equal to 0.07 A. The power of the lamp is equal to 2,247 W but the efficiency has to be taken into account. The effective power achieved by the mixture is consequently lower.

The second setup was similar to the first one but the distance between the mixture and the lamp was in this case 12 cm. This configuration was done to make sure, more of the radiation would hit the mixture. This because of the radiation angle of the lamp of 115 °.

The final setup consisted of a LED-lamp connected to two constant current LED-drivers serialized. In this case the distance between the mixture and the lamp was kept at 12 cm. By the use of the constant current LED-drivers, the power of the lamp was equal to its maximal power of 40 W. Also, in this case the efficiency of the lamp has to be taken into consideration.

### 3.2.2 Setup Monolith reactor

The batch reactor is replaced by the monolith reactor, when degradation in the batch reactor is measured. As mentioned earlier, the reactor is made by a 3D-printer. The monolith consists of sixteen channels with a diameter of 2 mm. The length of one channel is 150 mm and the distance between two channels is equal to 4 mm.

The CREE HighPower LED-lamp is also used in this case to illuminate the mixture and get its power from the two constant current LED-drivers. The settings of the LED-converters are set in such a way that the LED can deliver its maximum power of 40 W. Taking into consideration the efficiency of the lamp, the total power reaches the mixture is lower.

Because degradation is measured in the batch reactor, these mixtures are also used in the monolith reactor. The mixture consists of 0.1 mM DCF and 0.1 g/L Au/$TiO_2$ mixed into ultrapure water. This suspension is brought into a beaker and placed onto a stirring plate in the dark. The diaphragm liquid transfer pump brings this mixture to the top of the monolith reactor and the reacted mixture is received in a beaker under the reactor. To remove the catalyst, the 0.45 µm filters are used. In this case, the mixture is not measured after several hours but after several minutes. The setup of a similar setup is shown in Figure 14.

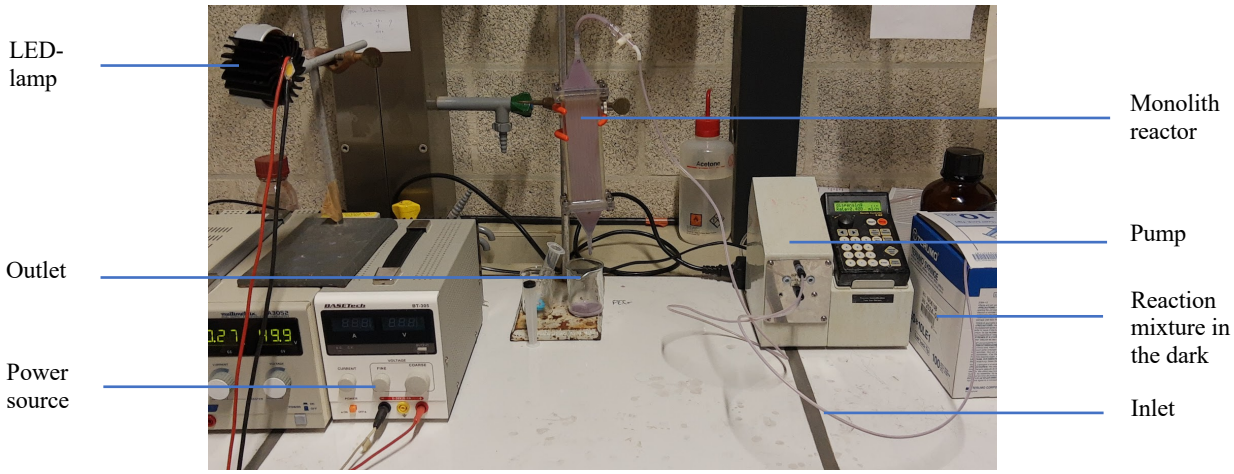


Figure 14: Setup monolith reactor (the power source and the pump are different than the described setup)

### 3.2.3 Analytic method

The first thing to do, is measuring the spectrum of DCF to get knowledge about its maximal absorption. The spectrum of DCF is measured with a concentration of 0.2 mM within 250 nm and 800 nm. For this experiment, the UV/VIS spectrophotometer is used. When the maximal absorption is known, the wavelength can be set to measure the degradation of DCF.

Before the degradation can be measured, a series of standards of DCF has to be made. This is necessary to measure the degradation of DCF after the spectrophotometric analysis. The series of standards is measured with the UV/VIS spectrophotometer with the maximal absorption of DCF, 276 nm. The series of standards is shown in Table 2 and at each dilution step the dilution factor (DF) is mentioned. There is started with a concentration of DCF of 0.4 mM.

Table 2: The series of standards of DCF with a starting concentration of 0.4 mM

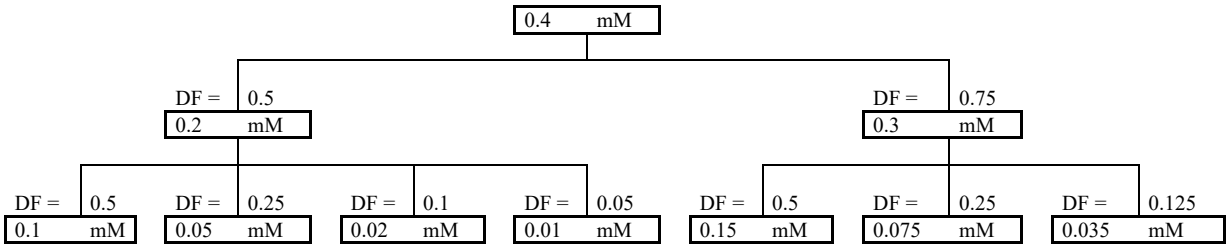


Another matter that has to be researched before starting the actual experiments is the difference between the absorption spectra of $Au/TiO_2$ and $TiO_2$. This will be reached by measuring each absorption spectrum within 200 nm and 800 nm. Each catalyst has a starting concentration of 0.2 g/L. These spectra are also measured by using the UV/VIS spectrophotometer.

Also, a series of standards of the catalyst $Au/TiO_2$ is made to detect its molar extinction coefficient. The starting concentration of $Au/TiO_2$ is 2 g/L. The UV/VIS spectrophotometer is in this case also used to monitor the absorption spectra of the different concentrations. The series of standards is shown in Table 3.

Table 3: The series of standards of $Au/TiO_2$ with a starting concentration of 2 g/L

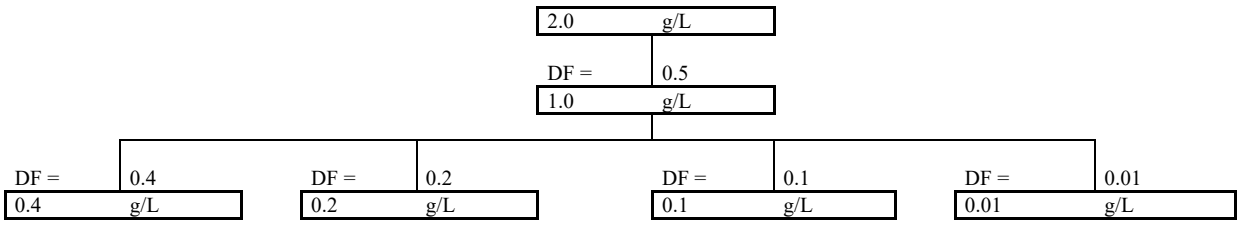


Now, the actual degradation experiments can start. As mentioned before, the degradation of DCF is first measured with the UV/VIS spectrophotometer. The whole absorption spectrum of the solution is studied to see of some degradation products are formed. It is possible that these products absorb light at the same wavelength as DCF. But when it absorbs light at a different wavelength it will be visible in the absorption spectrum. The 3 setups and the monolith setup will be discussed. When degradation is observed with the UV/VIS spectrophotometer there is switched to the HPLC.

HPLC is used to monitor the degradation of DCF and to detect the degradation products. As mentioned earlier, the stationary phase consists of a non-polar C18 column. An isocratic mobile phase, 40 % of methanol and 60 % of ammonium acetate 0.1 mM is used. 0.20 µL of the degradation mixture is pumped through the column with a flow rate of 0.800 mL/min. The absorption is measured at a wavelength of 276 nm.

When the degradation of DCF is detected in the monolith reactor and when the reaction products are identified, the degradation of DCF will be optimized. This by varying the catalyst concentration, flow rate and light intensity.

# 4 Results

## 4.1 Spectrum of DCF

### 4.1.1 Results and calculations

To detect the spectrum of DCF, a concentration of 0.2 mM is used. In the lab, 0.0337 g of DCF was weighed and was diluted to 500 mL with ultrapure water.

$$\frac{0.0337\ \text{g}}{500\ \text{mL}} \cdot 2 = 0.0674\ \text{g/L}$$

$$\frac{0.0674\ \text{g/L}}{296.148\ \text{g/mol}} = 0.000228\ \text{mol/L}$$

$$0.000228\ \text{mol/L} = 0.228\ \text{mmol/L (mM)}$$

The concentration present in the sample is equal to 0.228 mM. The spectrum is measured within the wavelengths 250 nm and 800 nm. The spectrum of DCF is shown in Figure 15 and details of the maximal absorption are shown in Table 4.

Table 4: Details about the maximal absorption of DCF

| Wavelength (nm) | Absorption |
|---|---|
| 270 | 2.135 |
| 271 | 2.171 |
| 272 | 2.200 |
| 273 | 2.214 |
| 274 | 2.225 |
| 275 | 2.232 |
| 276 | 2.233 |
| 277 | 2.233 |
| 278 | 2.224 |
| 279 | 2.210 |
| 280 | 2.188 |
| 281 | 2.162 |
| 282 | 2.130 |
| 283 | 2.093 |
| 284 | 2.050 |
| 285 | 1.990 |

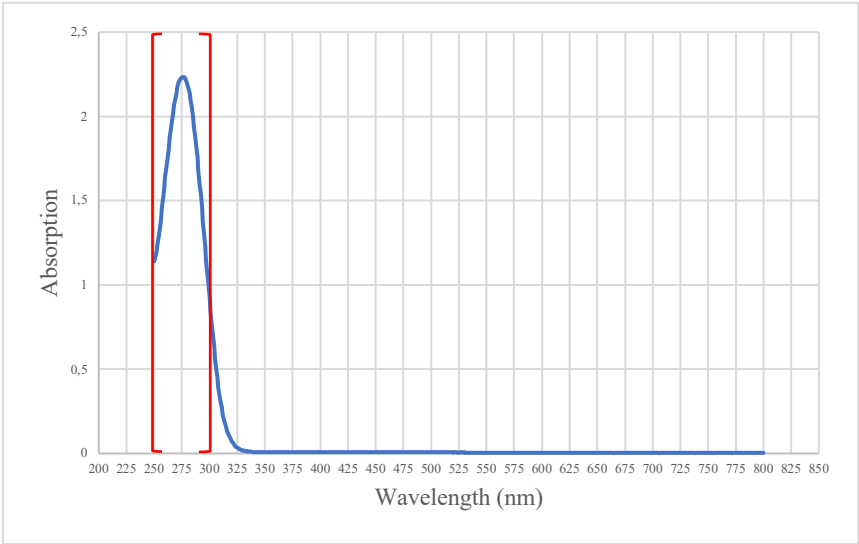


Figure 15: The absorption spectrum of DCF (0.228 mM)

### 4.1.2 Discussion

The spectrum of DCF was measured within 250 nm and 800 nm. In Figure 15, a peak is visible between the wavelengths of 250 nm and 300 nm. When Table 4 is observed, the maximal absorption is detected at 276 nm and 277 nm. There can be concluded that the maximal absorption of DCF is equal to 276 nm. At this wavelength, DCF absorbs most light. This is in line with previous studies [21], [31], [44].

## 4.2 Series of standards of DCF

### 4.2.1 Results and calculations

The starting concentration of DCF to make the series of standards is 0.4 mM. Therefore, 7.1 mg was weighed and was diluted to 50 mL with ultrapure water.

$$\frac{7.1\ \text{mg}}{50\ \text{mL}} \cdot 20 = 142\ \text{mg/L}$$

$$\frac{142 \cdot 10^{-3}\ \text{g/L}}{296.148\ \text{g/mol}} = 0.000479\ \text{mol/L}$$

$$0.000479\ \text{mol/L} = 0.479\ \text{mmol/L (mM)}$$

The updated series of standards of DCF is shown in Table 5. The starting concentration is 0.479 mM.

Table 5: The updated series of standards of DCF with a starting concentration of 0.479 mM

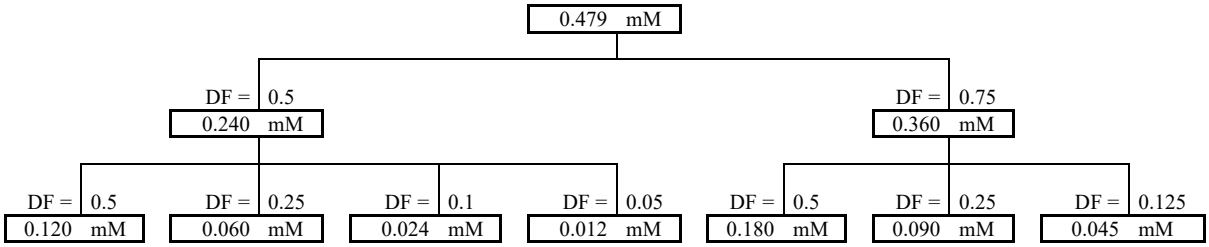


The absorption of each standard is measured at a wavelength op 276 nm. The results are present in Table 6.

Table 6: Results of spectrophotometric analysis of the series of standards of DCF with a starting concentration of 0.479 mM

| Absroption (276 nm) | Concentration (mM) |
|---|---|
| 0 | 0 |
| 0.109 | 0.012 |
| 0.232 | 0.024 |
| 0.424 | 0.045 |
| 0.582 | 0.060 |
| 0.819 | 0.090 |
| 1.150 | 0.120 |
| 1.722 | 0.180 |
| 2.209 | 0.240 |
| 3.140 | 0.360 |
| 3.481 | 0.479 |

A regression analysis is performed to measure the R square. Also, the coefficients are measured to establish the equation of the calibration line. These results are shown in Table 7.

Table 7: Results of the regression analysis of the results of the spectrophotometric analysis

| SUMMARY OUTPUT | |
|---|---|
| *Regression Statistics* | |
| Multiple R | 0.999 |
| R Square | 0.998 |
| Adjusted R Square | 0.997 |
| Standard Error | 0.054 |
| Observations | 10 |

ANOVA

| | *df* | *SS* | *MS* | *F* | *Significance F* |
|---|---|---|---|---|---|
| Regression | 1 | 9.469 | 9.469 | 3209.491 | $1.046 \cdot 10^{-11}$ |
| Residual | 8 | 0.024 | 0.003 | | |
| Total | 9 | 9.493 | | | |

| | *Coefficients* | *Standard Error* | *t Stat* | *P-value* | *Lower 95%* | *Upper 95%* | *Lower 95.0%* | *Upper 95.0%* |
|---|---|---|---|---|---|---|---|---|
| Intercept | 0.0362 | 0.0247 | 1.468 | 0.180 | -0.021 | 0.093 | -0.021 | 0.093 |
| X Variable 1 | 8.873 | 0.157 | 56.652 | $1.046 \cdot 10^{-11}$ | 8.512 | 9.234 | 8.512 | 9.234 |

The R square is equal to 0.998.

The equation of the calibration curve is of the form $y = a \cdot x + b$ with a equal to 8.873 and b equal to 0.0362. It follows $y = 8.873 \cdot x + 0.0362$ with y = absorption and x = concentration (mM).

As mentioned before, Lambert-Beer's law is equal to $E = \varepsilon\ c\ d$. Also, a is equal to $\varepsilon\ d$. For this test, cuvettes with a path length of 1 cm are used which means a is equal to ε, so ε is equal to 8.873 ($L\ mol^{-1}\ cm^{-1}$).

The results are based on 10 standards instead of 11. The standard 0.4 mM showed a different result and was therefore not taken into account.

These results of the spectrophotometric analysis and the calculations are shown in Figure 16.

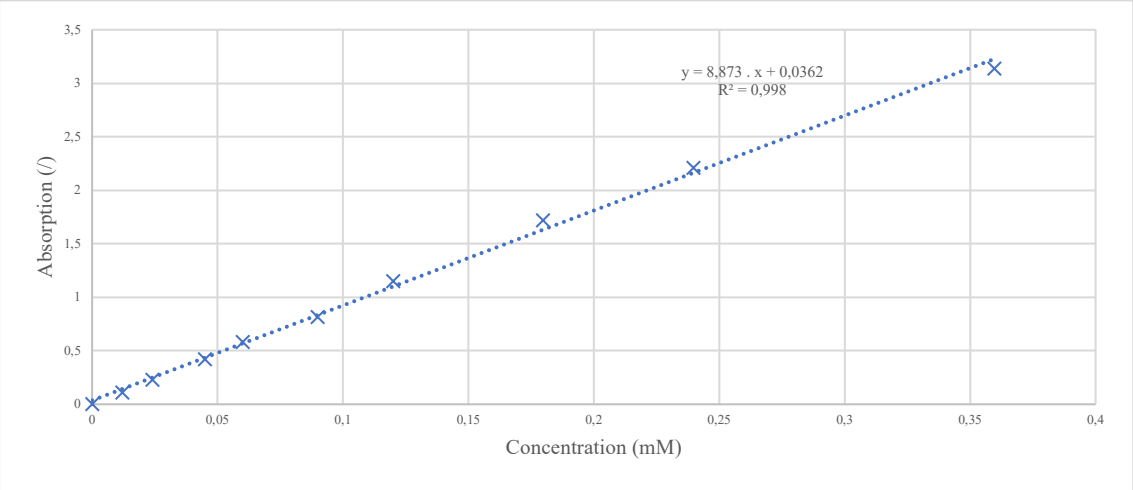


Figure 16: Visualization of the results of the spectrophotometric analysis at a wavelength of 276 nm and the regression analysis of the series of standards of DCF

### 4.2.2 Discussion

There are no major outliers on the calibration line instead of the standard 0.4 mM. So, this point was not taken into consideration. All the other measured points are very close to the calculated line. $R^2$ is 0.998. It is decided that R square is acceptable, and this series of standards can be used further. The equation of the calibration line is equal to absorption = 8.873 · concentration + 0.0362.

## 4.3 Equation spectra of $Au/TiO_2$ and $TiO_2$

### 4.3.1 Results and calculations

For both catalysts a solution of 0.2 g/L was made. Further, 0.028 g of $Au/TiO_2$ was weighed and diluted to 100 mL with ultrapure water.

$$\frac{0.0280\ \text{g}}{100\ \text{mL}} \cdot 10 = 0.280\ \text{g/L}$$

$Au/TiO_2$ has a molar mass of 80.83 g/mol.

$$\frac{0.280\ \text{g/L}}{80.83\ \text{g/mol}} = 0.00346\ \text{mol/L (M)}$$

For the catalyst $TiO_2$, 0.0386 g was weighed and diluted to 200 mL with ultrapure water.

$$\frac{0.0386\ \text{g}}{200\ \text{mL}} \cdot 5 = 0.193\ \text{g/L}$$

The molar mass of $TiO_2$ is equal to 79.66 g/mol.

$$\frac{0.193\ \text{g/L}}{79.66\ \text{g/mol}} = 0.00242\ \text{mol/L (M)}$$

The spectrum of $Au/TiO_2$ with a concentration of 0.00346 M is measured within the wavelengths 200 nm and 800 nm. The results of the spectrophotometric analysis are shown in Table 8. For each absorption, the molar extinction coefficient is measured, based on Lambert-Beer's law: $\frac{E}{c\ d} = \varepsilon$ with d = 1 cm. This in order to be able to make a good comparison between the two catalysts afterwards because different numbers of mole per liter were used. Figure 17 shows the spectrum of $Au/TiO_2$ with on the y-axis the molar extinction coefficient (L $mol^{-1}$ $cm^{-1}$) and on the x-axis the wavelength (mM).

Table 8: Results of the spectrophotometric analysis of $Au/TiO_2$

| Wavelength (nm) | Absorption | Molar extinction coefficient (L $mol^{-1}$ $cm^{-1}$) |
|---|---|---|
| 200 | 1.442 | 416.29 |
| 250 | 1.429 | 412.54 |
| 300 | 1.496 | 431.84 |
| 350 | 1.546 | 446.31 |
| 400 | 1.456 | 420.33 |
| 450 | 1.361 | 392.91 |
| 500 | 1.267 | 365.77 |
| 550 | 1.182 | 341.23 |
| 600 | 1.098 | 316.98 |
| 650 | 1.019 | 294.17 |
| 700 | 0.944 | 272.52 |
| 750 | 0.880 | 254.05 |
| 800 | 0.827 | 238.75 |

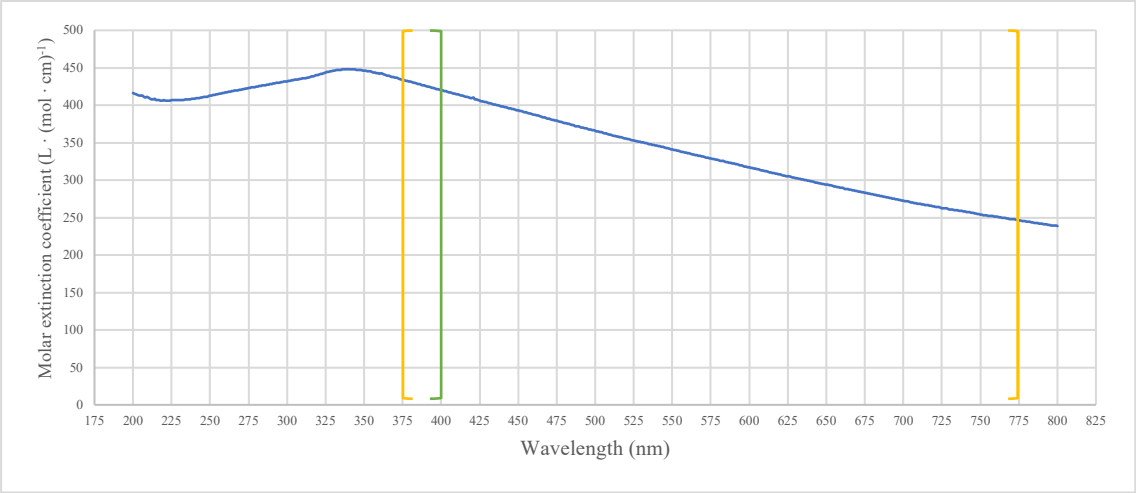


Figure 17: The absorption spectrum of Au/$TiO_2$ (0.00346 M)

The spectrum of $TiO_2$ with a concentration of 0.00242 M is also measured within the wavelengths 200 nm and 800 nm. The results of this spectrophotometric analysis are shown in Table 9. In this case, the molar extinction coefficient is also measured to be able to make a good comparison between the two catalysts. The spectrum of $TiO_2$ is shown in Figure 18.

Table 9: Results of the spectrophotometric analysis of $TiO_2$

| Wavelength (nm) | Absorption | Molar extinction coefficient (L $mol^{-1}$ $cm^{-1}$) |
|---|---|---|
| 200 | 4.504 | 1859.01 |
| 250 | 4.945 | 2041.03 |
| 300 | 4.985 | 2057.54 |
| 350 | 3.478 | 1435.53 |
| 400 | 2.215 | 914.23 |
| 450 | 1.790 | 738.82 |
| 500 | 1.476 | 609.21 |
| 550 | 1.247 | 514.69 |
| 600 | 1.072 | 442.46 |
| 650 | 0.936 | 386.33 |
| 700 | 0.832 | 343.40 |
| 750 | 0.747 | 308.32 |
| 800 | 0.675 | 278.60 |

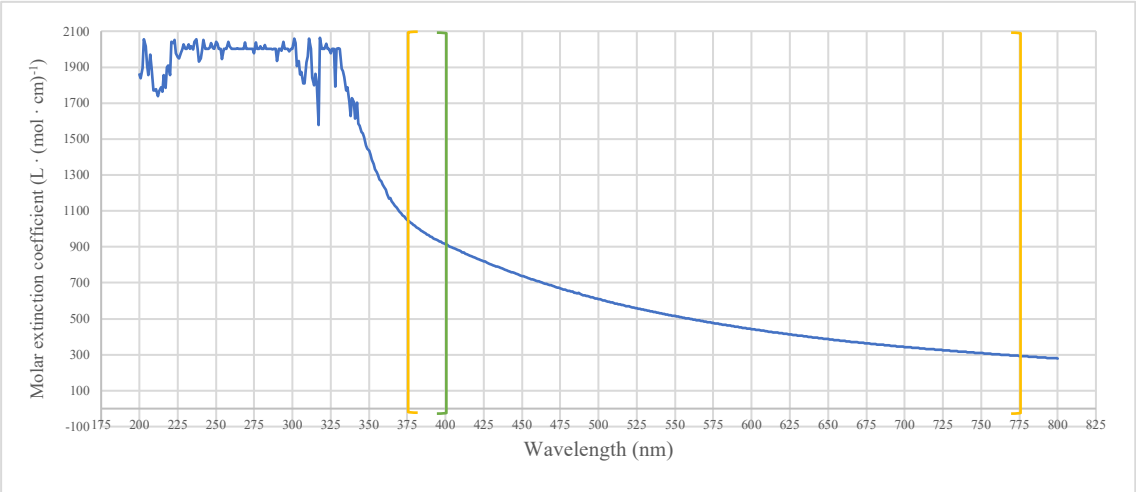


Figure 18: The absorption spectrum of $TiO_2$ (0.00242 M)

### 4.3.2 Discussion

The molar extinction coefficient was obtained from the UV-VIS data to compare $TiO_2$ and $Au/TiO_2$. The UV-spectrum ranges from 10 nm to 400 nm. This is shown in Figure 17 and Figure 18 with the use of green lines. The VIS-spectrum (380 nm to 780 nm) is visualized in Figure 17 and Figure 18 with yellow lines. As mentioned before, gold is added to the catalyst to widen the absorption spectrum of the catalyst. In this case, the catalysts $TiO_2$ (Degussa) and $Au/TiO_2$ (Aurolite) are used.

When there is looked at the spectrum of $Au/TiO_2$ there can be concluded that the molar extinction coefficient is between 450 and 250 (L $mol^{-1}$ $cm^{-1}$). The lowest extinction coefficient measured is equal to 238.75 (L $mol^{-1}$ $cm^{-1}$) at a wavelength of 800 nm. The maximal molar extinction coefficient is reached at a wavelength around 350 nm.

When the results of the spectrum of $TiO_2$ are studied, there can be concluded that the maximal molar extinction coefficient is reached at a wavelength around 300 nm. The minimal molar extinction coefficient is reached at a wavelength of 800 nm.

The overall conclusion is that $Au/TiO_2$ during the whole spectrum is under the spectrum of $TiO_2$. This can be explained by the use of $TiO_2$ (Degussa). A study explains that the molar extinction coefficient of a catalyst with the use of Degussa is much higher than those with a different oxide [45]. These experiments cannot conclude that $Au/TiO_2$ (Aurolite) has a wider absorption spectrum in comparison with $TiO_2$ (Degussa). Further, research have to be done where experiments has to be set up to measure the band gaps of each catalyst.

## 4.4 Series of standards of $Au/TiO_2$

### 4.4.1 Results and calculations

The starting concentration of $Au/TiO_2$ to make the series of standards is 0.2 g/L. Because of its bad solubility, the series of standards is made with a starting concentration of 0.1 g/L. The sample with a concentration of 0.2 g/L is also measured but is not used to make the series of standards to avoid unreliable results. Further, 0.1907 g of $Au/TiO_2$ was weighed and diluted to 100 mL with ultrapure water.

$$\frac{0.1907\ \text{g}}{100\ \text{mL}} \cdot 10 = 1.907\ \text{g/L}$$

For the series of standards, 0.1036 g $Au/TiO_2$ was weighed and diluted to 100 mL.

$$\frac{0.1036\ \text{g}}{100\ \text{mL}} \cdot 10 = 1.036\ \text{g/L}$$

The updated series of standards is shown in Table 10 with a starting concentration of 1.036 g/L and a concentration of 1.907 g/L.

Table 10: The updated series of standards of $Au/TiO_2$ with a starting concentration of 1.036 g/L and a concentration of 0.1907 g/L

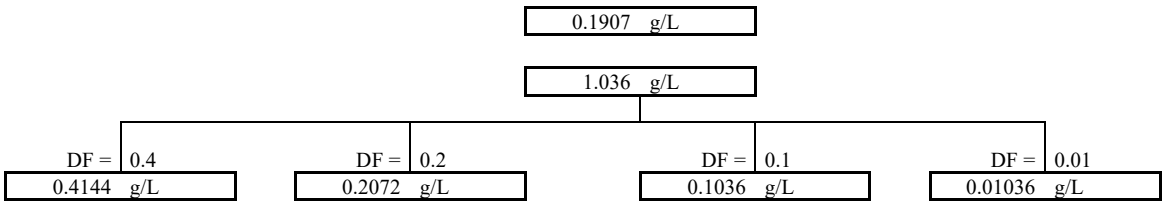


For each standard, the whole absorption spectrum is measured within the wavelengths 250 nm and 800 nm. The spectra are shown in Figure 19. Around a wavelength of 328 nm, the maximal absorption is

detected. But only for the standards 0.2 g/L, 0.1 g/L and 0.01 g/L realistic results are obtained. The standards 2 g/L, 1 g/L and 0.4 g/L have a concentration which is too high.

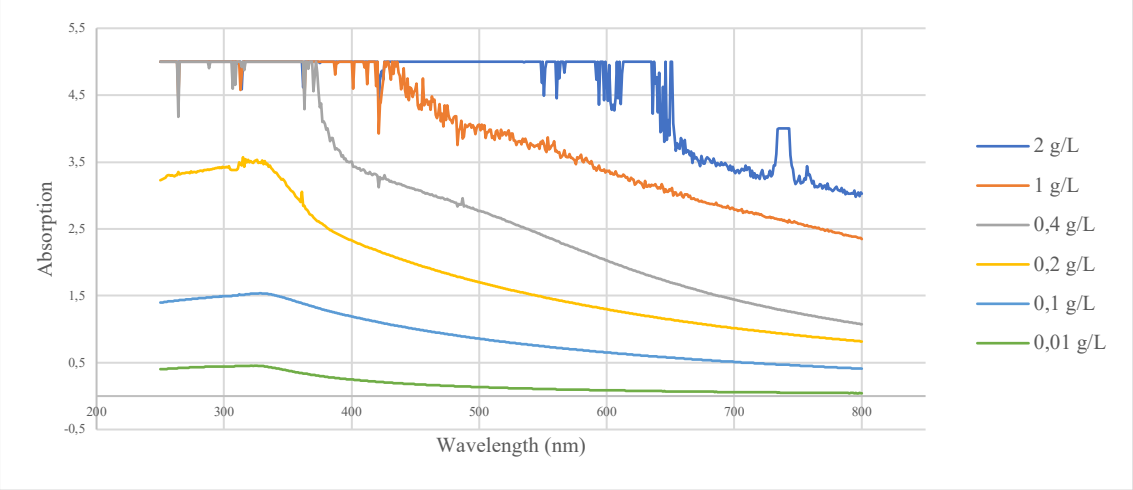


Figure 19: The absorption spectra of the standards of $Au/TiO_2$

The molar mass of $Au/TiO_2$ is equal to 80.83 g/mol. So, the concentration in M can be measured. Next, the molar extinction coefficient can be measured with the Lambert-Beer's law: $\frac{E}{c\ d} = \varepsilon$ with d = 1 cm. These results of the spectrophotometric analysis and calculation are shown in Table 11.

Table 11: Results of the spectrophotometric analysis at a wavelength of 328 nm and calculations

| Concentration (g/L) | Concentration (M) | Absorption (/) | Molar extinction coefficient (L $mol^{-1}$ $cm^{-1}$) |
|---|---|---|---|
| 0.2072 | 0.00256 | 3.494 | 1375.18 |
| 0.1036 | 0.00128 | 1.538 | 1200.01 |
| 0.01036 | 0.000128 | 0.452 | 3542.30 |

There is a big difference between the results of 0.2 g/L and 0.1 g/L, and 0.01 g/L. The results are interpreted on the basis of those of 0.2 g/L and 0.1 g/L. The average molar extinction coefficient is equal to 1287.59 (L $mol^{-1}$ $cm^{-1}$).

### 4.4.2 Discussion

The molar extinction coefficients of the standards: 2 g/L, 1 g/L and 0.4 g/L cannot be measured because it reached the maximal absorption. When there is looked at the other molar extinction coefficients there can be concluded that only the values of 0.2 g/L and 0.1 g/L are around the same value. Out of these results can be derived that the molar extinction coefficient is equal to 1287.59 (L $mol^{-1}$ $cm^{-1}$).

But out of the previous experiment can be deduced that the molar extinction coefficient is equal to 446.31 (L $mol^{-1}$ $cm^{-1}$) for a solution of 0.28 g/L. This can be explained by the negative deviation from Lambert-Beer's law. This is caused by a concentration which is too high. This results in an interaction between the catalysts, which causes the absorption characteristics to be affected. Another reason is that refractive index is changed by the high concentration causing abnormalities to be observed in Lambert-Beer's law [46].

Another explanation of the different molar extinction coefficients can be the inaccurate operation during the setting up of the series of standards. During the production of the series of standards was observed that the catalyst did not fully dissolve. The production of a new standard out of a previous standard, there may be inaccuracies that may explain the difference in molar extinction coefficients.

When there is the possibility, the series of standards has to be made again. In this case, every standard has to be weighed, so no inaccuracies can occur.

## 4.5 Experiment 1

### 4.5.1 Results and calculations

This experiment consists of three reactors. The first one contained 0.1 mM DCF and 0.1 g/L Au/$TiO_2$ mixed in ultrapure water. Then, 0.0337 g DCF was weighed and diluted to 500 mL with ultrapure water. This is equal to 0.228 mM. For Au/$TiO_2$, 0.028 g was weighed and diluted to 100 ml so equal to 0.28 g/L. The total reaction volume was 100 mL consisting of 50 mL DCF solution and 50 mL Au/$TiO_2$ solution. Both solutions were diluted with a DF of 0.5. The reaction mixture consisted of 0.114 mM DCF and 0.14 g/L Au/$TiO_2$. This mixture was made two times, one was placed in the dark and the other one was placed under the LED-lamp that is positioned 20 cm above the solution. The power that reaches the mixture was generated by the Basetech BT-305. The third reactor contained only DCF. The 50 mL 0.228 mM DCF solution was diluted with 50 mL ultrapure water. This mixture was also placed under the light source.

After several hours the samples were measured with the UV/VIS spectrophotometer at a wavelength of 276 nm. At the beginning two samples were taken: one with a 0.45 µm filter and one without. Based on the comparison obtained from the series of standards, $\frac{absorption-0.0362}{8.873}$ = concentration (mM), the concentration of DCF can be measured. The results of these experiments are shown in Table 12 and Table 13.

Table 12: Results of the spectrophotometric analysis (276 nm) and calculations of samples with and without a 0.45 µm filter

| | | DCF, Au/$TiO_2$, Light | DCF, Light | DCF, Au/$TiO_2$, Dark |
|---|---|---|---|---|
| With 0,45 µm filter | Absorption (/) | 1.162 | 1.110 | 1.113 |
| | Concentration (mM) | 0.127 | 0.121 | 0.121 |
| Without filter | Absorption (/) | 1.797 | 1.123 | 1.967 |
| | Concentration (mM) | 0.198 | 0.122 | 0.218 |

Table 13: Results of the spectrophotometric analysis (276 nm) and calculation of samples taken after several hours of experiment 1

| | | DCF, Au/$TiO_2$, Light | DCF, Light | DCF, Au/$TiO_2$, Dark |
|---|---|---|---|---|
| Start | Absorption (/) | 1.162 | 1.110 | 1.113 |
| | Concentration (mM) | 0.127 | 0.121 | 0.121 |
| After 1 h | Absorption (/) | 1.156 | 1.118 | 1.125 |
| | Concentration (mM) | 0.126 | 0.122 | 0.123 |
| After 2 h | Absorption (/) | 1.158 | 1.125 | 1.118 |
| | Concentration (mM) | 0.126 | 0.123 | 0.122 |
| After 3 h | Absorption (/) | 1.149 | 1.134 | 1.102 |
| | Concentration (mM) | 0.125 | 0.124 | 0.120 |
| After 24 h | Absorption (/) | 1.062 | 1.383 | 1.135 |
| | Concentration (mM) | 0.116 | 0.152 | 0.124 |

### 4.5.2 Discussion

When the results of the experiment with and without filter are studied, clear conclusions can be made. When looking at the two different samples, with and without filter, of DCF, Au/$TiO_2$ in the light and

DCF, $Au/TiO_2$ in the dark, big differences in concentrations are found. However, when studying the results of the sample consisting only DCF in the light, the same concentrations are detected. There can be concluded that the 0.45 µm filter does not eliminate DCF out of the sample. Studying the results of the two different samples with filter of DCF, $Au/TiO_2$ in the light and DCF, $Au/TiO_2$ in the dark in comparison with the sample DCF in the light, about the same concentrations are found. There can be deduced that the 0.45 µm filter eliminates the catalyst. This filter can be used for the further experiments.

When the results of the degradation are studied there can be concluded that the results are stable except for a few values. The concentration of DCF, $Au/TiO_2$, light after 24 hours has a really low concentration. This can be explained by the degradation of DCF or an unreliable measurement. Further experiments have to explain this result. The other deviating result is DCF, light after 24 hours. The concentration is very high in comparison with the other results. This can be clarified by the contamination of the cuvette.

Overall, there can be concluded that degradation of DCF has not taken place. This can be the result of the low amount of radiation that reaches the mixture. So, no photocatalytic reaction can take place.

## 4.6 Experiment 2

### 4.6.1 Results and calculations

In this case, the experiment consists also of three reactors. For DCF the same standard was used as in the first experiment. The concentration was equal to 0.228 mM. The $Au/TiO_2$ solution consisted of 0.019 g $Au/TiO_2$ diluted with ultrapure water to 100 mL. The concentration was equal to 0.190 g/L. Those reagents were diluted with a DF of 0.5 so each sample consisted of 0.114 mM DCF and 0.095 g/L $Au/TiO_2$. The samples in the light were placed under the LED-lamp and the distance between the mixture and the lamp is equal to 12 cm. The lamp was connected to Basetech BT-305.

The samples were measured after several hours with the UV/VIS spectrophotometer at a wavelength of 276 nm. The concentration of DCF can be measured with the comparison obtained from the series of standards, $\frac{absorption-0.0362}{8.873}$ = concentration (mM). These results are shown in Table 14. Different with the experiment before, the whole spectrum of the samples consisting of DCF and $Au/TiO_2$ placed in the light were measured within 200 nm and 350 nm. These spectra are shown in Figure 20.

Table 14: Results of the spectrophotometric analysis (276 nm) and calculation of samples taken after several hours of experiment 2

| | | DCF, $Au/TiO_2$, Light | DCF, Light | DCF, $Au/TiO_2$, Dark |
|---|---|---|---|---|
| Start | Absorption (/) | 1.099 | 1.078 | 1.109 |
| | Concentration (mM) | 0.120 | 0.117 | 0.121 |
| After 1 h | Absorption (/) | 1.121 | 1.093 | 1.137 |
| | Concentration (mM) | 0.122 | 0.119 | 0.124 |
| After 2 h | Absorption (/) | 1.132 | 1.135 | 1.180 |
| | Concentration (mM) | 0.123 | 0.124 | 0.129 |
| After 24 h | Absorption (/) | 1.351 | 1.162 | 1.162 |
| | Concentration (mM) | 0.148 | 0.127 | 0.127 |

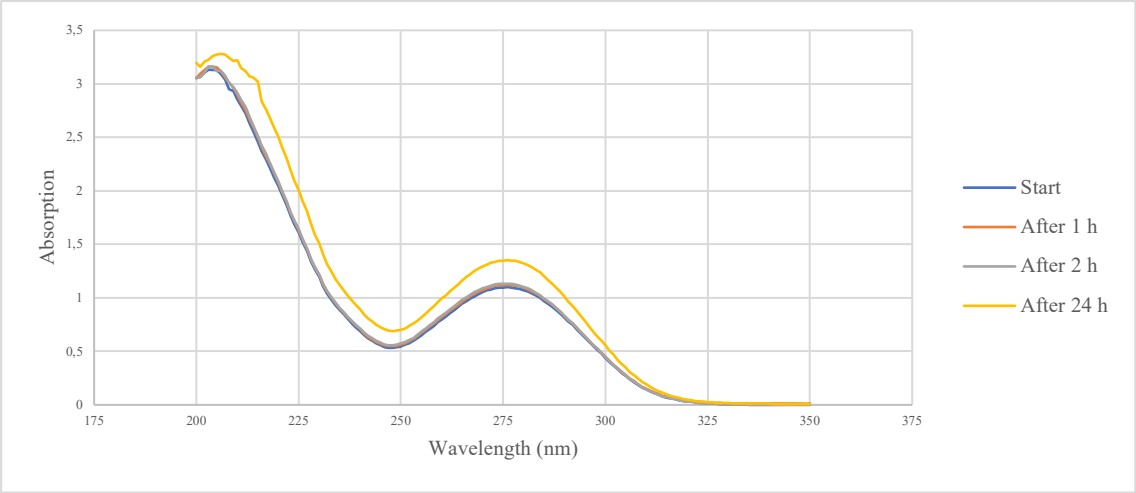


Figure 20: The absorption spectra of the sample consisting DCF and $Au/TiO_2$ placed under the LED-lamp after several hours of experiment 2

### 4.6.2 Discussion

For the three samples can be concluded that the concentration of DCF increases within the hours. This is also visualized in Figure 20. This can be clarified by the production of degradation products that absorb at the same wavelength as DCF. However, these products have higher concentrations or can absorb more light in comparison with the same amount of DCF. But these possible degradation products cannot be identified with the UV/VIS spectrophotometer. There has to be switched to a HPLC analysis.

The results of DCF, light and DCF, $Au/TiO_2$, dark are stable which means, no degradation took place.

## 4.7 Experiment 3

### 4.7.1 Results and calculations based on a spectrophotometric analysis

The setup was the same as experiment 2 but in this case, the lamp was connected to two constant current LED-drivers. In this experiment, the same standard of DCF was used as in experiment 1. The concentration was equal to 0.228 mM. The standard of $Au/TiO_2$ was made by weighing 0.0215 g $Au/TiO_2$ and diluting with ultrapure water to 100 mL. The concentration was equal to 0.215 g/L. The three same reactors were set up as described in the previous experiments. The reactors consisted of 0.114 mM DCF and 0.108 g/L $Au/TiO_2$.

The results are measured similar to experiment 2. The results and calculations of the spectrophotometric analysis are present in Table 15. The spectra measured within 200 nm and 350 nm of the samples consisting of DCF and $Au/TiO_2$ placed in the light are shown in Figure 21.

Table 15: Results of the spectrophotometric analysis (276 nm) and calculation of samples taken after several hours of experiment 3

| | | DCF, $Au/TiO_2$, Light | DCF, Light | DCF, $Au/TiO_2$, Dark |
|---|---|---|---|---|
| Start | Absorption (/) | 1.098 | 1.093 | 1.097 |
| | Concentration (mM) | 0.120 | 0.119 | 0.120 |
| After 1 h | Absorption (/) | 1.203 | 1.174 | 1.142 |
| | Concentration (mM) | 0.131 | 0.128 | 0.125 |
| After 2 h | Absorption (/) | 1.116 | 1.199 | 1.144 |
| | Concentration (mM) | 0.122 | 0.131 | 0.125 |
| After 3 h | Absorption (/) | 1.198 | 1.189 | 1.103 |

| | | | | |
|---|---|---|---|---|
| | Concentration (mM) | 0.131 | 0.130 | 0.120 |
| After 24 h | Absorption (/) | 1.252 | 1.123 | 1.145 |
| | Concentration (mM) | 0.137 | 0.122 | 0.125 |

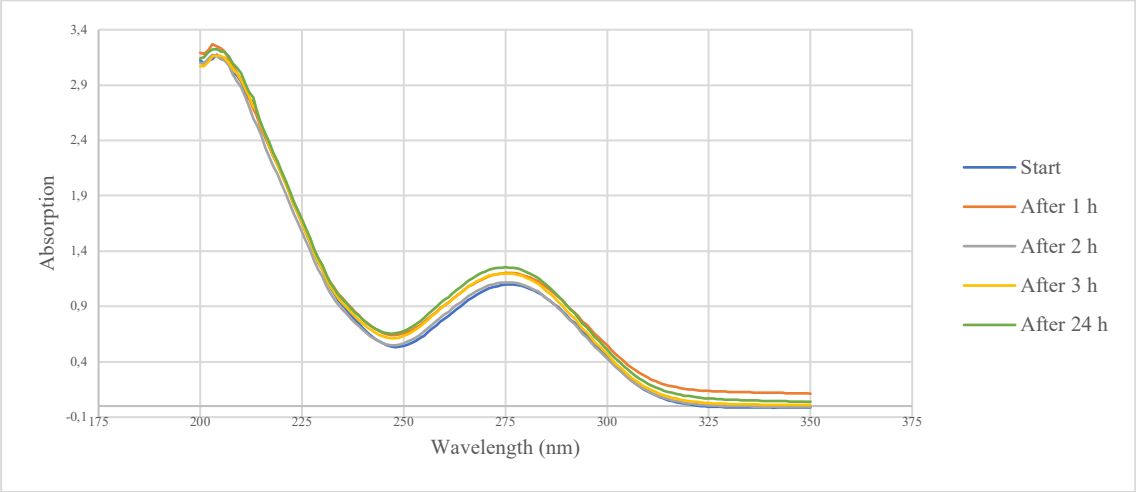


Figure 21: The absorption spectra of the sample consisting DCF and Au/$TiO_2$ placed under the LED-lamp after several hours of experiment 3

### 4.7.2 Discussion

It is shown in Table 15, that the concentration of DCF increases within the several hours. But the concentration of DCF in sample DCF, Au/$TiO_2$, light is really high after one hour. This can be explained by contamination of the cuvette. The concentrations of DCF in the samples of DCF, Au/$TiO_2$, dark and DCF, light are stable during the whole experiment. No degradation of DCF took place in these reactors.

Figure 21 shows that an increase of the concentration of DCF is detected. Only the sample after 1 hour shows a concentration not similar with the other concentrations. As mentioned before, these can be caused by contamination of the cuvette. The increase of the concentration can be explained by the production of degradation products. As explained in experiment 2, the spectrophotometric analysis cannot confirm this. A HPLC analysis is necessary to affirm this hypothesis.

### 4.7.3 Results and calculations based on a HPLC analysis

The same setup as described in 4.7.1 is examined. In this case, a HPLC analysis is performed after several hours. The isocratic mobile phase consists of 40 % of methanol and 60 % of ammonium acetate 0.1 mM. 0.20 µL of the degradation mixture is pumped through the column with a flow rate of 0.800 mL/min. The absorption is measured at a wavelength of 276 nm. The chromatograms are shown in Figure 22 and Figure 23.

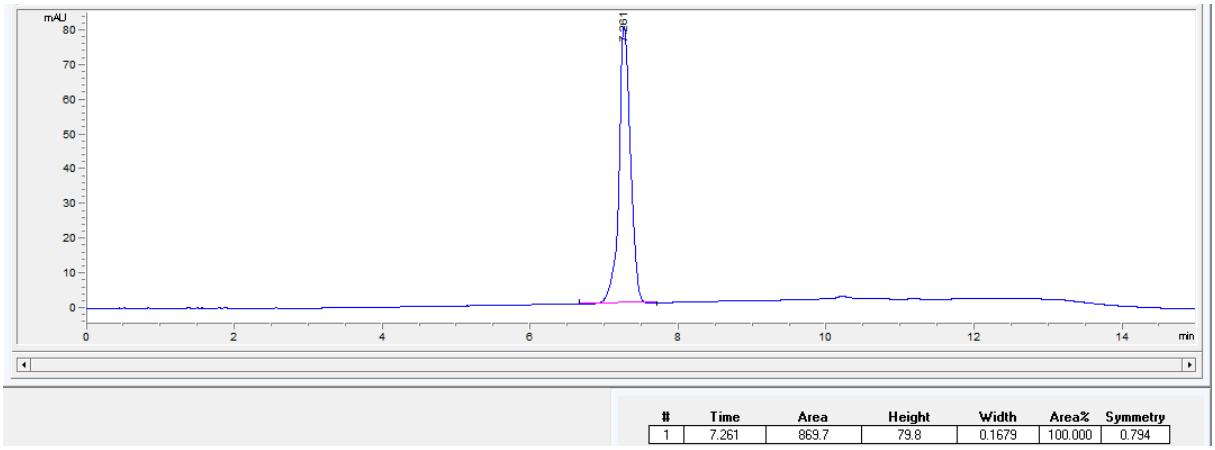


| # | Time | Area | Height | Width | Area% | Symmetry |
|---|---|---|---|---|---|---|
| 1 | 7.261 | 869.7 | 79.8 | 0.1679 | 100.000 | 0.794 |

Figure 22: The chromatogram of the starting solution consisting DCF and Au/$TiO_2$ placed in light

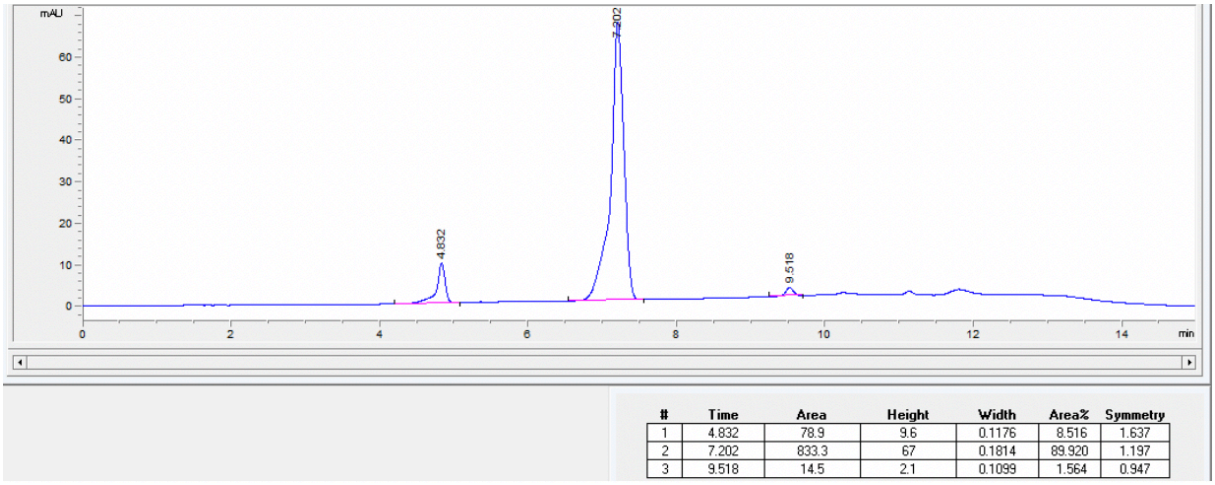


| # | Time | Area | Height | Width | Area% | Symmetry |
|---|---|---|---|---|---|---|
| 1 | 4.832 | 78.9 | 9.6 | 0.1176 | 8.516 | 1.637 |
| 2 | 7.202 | 833.3 | 67 | 0.1814 | 89.920 | 1.197 |
| 3 | 9.518 | 14.5 | 2.1 | 0.1099 | 1.564 | 0.947 |

Figure 23: The chromatogram of the solution consisting DCF and Au/$TiO_2$ placed in light after 4 hours

### 4.7.4 Discussion

In Figure 22 the chromatogram of the starting solution is shown. One peak is visible and presents DCF. It has a retention time of 7.261 minutes and the area under the curve is equal to 869.7. The second chromatogram presents the results of the solution DCF, Au/$TiO_2$, light radiated 4 hours. When studying this chromatogram, shown in Figure 23, three peaks can be observed. The second peak presents DCF. This can be concluded based on the retention time. The area under the curve is equal to 833.3. So, there can be analyzed that the concentration of DCF is decreased and a photocatalytic degradation reaction took place. The actual concentration of DCF cannot be measured because a series of standards was not yet made.

The two other peaks present the degradation products. The first peak has a retention time of 4.832 minutes and has an area under the curve of 78.9. The third peak is a really small peak and has a retention time of 9.518 minutes and has an area under the curve of 14.5. Based on this analysis cannot be concluded which degradation product this is or products these are. Studies show that there are eight reaction products with different retention times. To identify these products, a HPLC MS has to be done. Then, the concentration of each peak can also be measured. It seems like the total concentration is increased but there is no information of the concentration of each peak. The means that it is in fact possible that the products are present with higher concentrations in comparison with DCF. Or that these products may absorb more light. Further experiments have to clarify this lack of knowledge.

# 5 Conclusion

The main aim of this thesis is met. Photocatalytic degradation of DCF took place. The degradation was first observed when using the LED-lamp at a distance of 12 cm between the mixture and the lamp and connected to the Basetech BT-305. The degradation was also observed when connected to two constant current LED-drivers. First, the degradation was observed with the UV/VIS spectrophotometer by an increase of the concentration at a wavelength of 276 nm. This could be caused by the production of degradation products. Afterwards, this was confirmed by the HPLC analysis. The concentration of DCF was decreased and other peaks were formed. These peaks probably represent the degradation products.

# 6 Future

There can be concluded that degradation of DCF took place. But there is an absence of knowledge and there are still some experiments that have to be carried out in order to complete this subject.

First, the experiments with regard to the catalyst have to be repeated. Also, an experiment to measure the band gaps of the two different catalysts has to take place. So, there can be concluded if the addition of gold widens the absorption spectrum of the catalyst. This can be measured with the Tauc plot. Secondly, the series of standards have to be made again to detect the molar extinction coefficient of $Au/TiO_2$. This time by weighing each standard to avoid inaccuracies instead of making a standard out of a previous standard.

Second, experiment 1 has to be repeated. This because a lower concentration was detected after 24 hours. This is in contrast with experiment 2 and 3 where the concentration is higher at the end. When the concentration of experiment 1 is also higher after 24 hours, it means a mistake was made during the experiment. If the concentration is still lower after 24 hours a HPLC analysis has to be completed to analyze the sample.

Then the HPLC analysis must be further developed. Now, two new peaks were detected. By changing the settings maybe more peaks can be detected. This because some degradation products have a similar retention time. Right now, it is possible that these products leave the column at the same time. Changing the setting can make it possible to let them come out separately. To identify the degradation products a HPLC MS analysis has to be performed. So, this is a next step in the process.

When the reaction in the batch reactor is on point and the right settings for the HPLC analysis are installed, the batch reactor will be replaced by the monolith reactor. The setup of this experiment will be performed as subscripted in 3.2.2.

Last, as mentioned before, when the degradation of DCF is detected in the monolith, the degradation of DCF will be optimized. The catalyst concentration, flow rate and light intensity will be altered till the maximal degradation is observed.

# VALIDATION OF SIMULATIONS OF DIFFERENT MONOLITHS FOR PHOTOCHEMICAL REACTIONS

**Lotte Thys[1], Mathias Jacobs[2] and Mumin Enis Leblebici[2,3]**

[1] *University Hasselt & University of Leuven, Faculty of Engineering Technology, Agoralaan Building B & H, B-3590 Diepenbeek, Belgium*

[2] *KU Leuven, Department of Chemical Engineering, Sustainable Chemical Process Technology TC, Diepenbeek Campus, Research unit CIPT, Agoralaan Building B bus 8, B-3590 Diepenbeek, Belgium*

[3] *Process Engineering for Sustainable Systems, Department of Chemical Engineering, KU Leuven, Celestijnenlaan 200F Box 2424, B-3001 Leuven, Belgium*

## ABSTRACT

Photochemical reactions are commonly performed in batch reactors. However, these designs have two disadvantages: photon transfer limitations and mass transfer limitations. To solve these issues, microreactors can be used. To raise the productivity and energy efficiency, a monolith reactor can be created consisting of small channels placed parallel next to each other. Not a lot of studies have yet been published on the dimensioning of a translucent monolith reactor. This article focused on the development of productive and energy efficient monolith reactors. Multiple parameters were changed, and each reactor design was validated. First, the simulation software COMSOL was used to calculate ray tracing and computational fluid dynamics. These parameters gave information about the interaction between the light and the particle on the one hand and the throughput on the other. Second, out of these parameters the photochemical space-time yield was measured which reflected the amount of product produced by a volumetric specific yield per power and unit of time. The relative SD was calculated to evaluate the homogeneity of the light absorption and the throughput. The results show that the RSD, for both parameters, increases with the volume of the reactor. The PSTY also increases with a raise of the volume in comparison with the productivity.

**Keywords:** *Photochemistry, COMSOL, Ray tracing, CFD, PSTY.*

## INTRODUCTION

### PHOTOCHEMISTRY

A photochemical reaction occurs under the influence of light. Light consists of a bundle of photons that carry the energy in the form of electromagnetic radiation. When the target molecule absorbs the light, the energy of the photons is given to this molecule. Changes in the electrical structure of the molecule take place, so a reaction is possible. The molecule is now in an excited state. No source of heat is used to get this electron in excited state [4], [13].

The advantages of this technique are increased selectivity, mild reaction conditions and it has a low demand for organic solvents compared to thermochemical reactions. However, it has also some disadvantages. First, the reaction rate is very low when using conventional batch reactors and second, it usually has a low energy efficiency due to suboptimal reactor design [13].

Three fundamental events can be distinguished during a photochemical reaction:

1. first, the light has to be absorbed by the target molecule [10].
   The Lambert-Beer's law, shown in equation (6), dictates that the concentration ($c$) of the light-absorbing compound is directly proportional to the absorbance ($E$). The molar extinction coefficient ($\varepsilon$) can also be extracted from this law. This is the probability that the light is absorbed. The length ($d$) of the cuvette must also be taken into account [10], [18];

$$E = \varepsilon \; c \; d \tag{6}$$

2. second, it is crucial that the photon activates the molecule that has absorbed the photon [19];
3. the third law states that the total energy dose is directly proportional to the number of molecules produced [10].

In photochemistry, the quantum yield ($\Phi$) is a well know parameter. This is defined by the ratio of the number of molecules formed or decomposed to the number of photons absorbed by the reacted molecules. This can be calculated by equation (7) [47].

$$\Phi = \frac{\#\ molecules\ decomposed}{\#\ photons\ absorbed} \quad (7)$$

## SINGLET OXYGEN

Oxygen has eight electrons on which two electrons are unpaired. They have the same spin and are placed in different π orbitals, hence, the ground state of oxygen is a triplet state. It is a fairly stable molecule and can oxidize other molecules. But this oxidation reaction is kinetically slow caused by the spin of the unpaired electrons [48].

Further, by adding energy, the triplet ground state ($^3\Sigma_g^-$) converts to singlet oxygen ($^1\Delta_g$). The electron configuration makes singlet oxygen more reactive with 95 kJ $mol^{-1}$ more than the triplet state and increases the oxidation capacity. One unpaired electron jumps to the orbital of the other unpaired electron. The two electrons have an antiparallel spin. This molecule has a lifetime of $10^{-6}$ – $10^{-3}$ s in a solution which is much shorter than this of the triplet state [48], [49]. The phenomenon is shown in Figure 24.

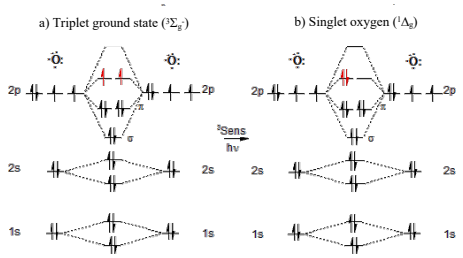


**Figure 24.** Schematic visualization of the atomic structures of: a) the triplet ground state of oxygen and b) of singlet oxygen [50]

To induce this transition, light with a wavelength of 1269 nm has to be absorbed or has to be emitted. With the addition of a photosensitizer this wavelength can be reduced. This is a specific molecule which absorbs a certain wavelength and generates singlet oxygen [49], [51].

When light is absorbed by the photosensitized it goes from ground state ($S_0$) to the excited single state ($S_1$). Next, intersystem crossing changes the single state ($S_1$) to the triplet state ($T_1$). This state has a longer lifetime which makes interaction with oxygen possible. Then the photosensitizer gives its energy to the triplet ground state of oxygen producing singlet oxygen [49], [52]. Figure 25 presents a schematic representation of this process.

$$\text{Photosensitizer} \xrightarrow{h\nu} {}^1\text{Photosensitizer*}$$

$$^1\text{Photosensitizer*} \longrightarrow {}^3\text{Photosensitizer*}$$

$$^3\text{Photosensitizer*} + O_2\ (^3\Sigma_g^-) \longrightarrow \text{Photosensitizer} + O_2\ (^1\Delta_g)$$

$$O_2\ (^1\Delta_g) + \text{substrate} \longrightarrow \text{Oxidation}$$

Rose Bengal is a commonly used photosensitizer and absorbs visible light with a wavelength between 480 nm and 550 nm. The sensitizer has a quantum yield of 0.76 in water [49].

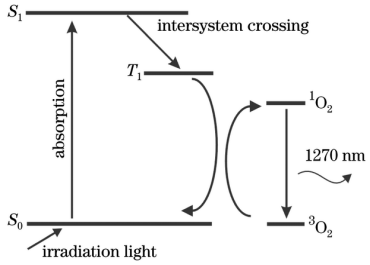


**Figure 25.** Illustration of the mechanism of action from a photosensitizer [53, p. 86]

As mentioned earlier, $O_2$ ($^1\Delta_g$) has a really short lifetime. But 9,10-diphenylanthracene (DPA) is an acceptor for $O_2$ ($^1\Delta_g$) which forms an endoperoxide ($DPAO_2$). This endoperoxide is used to detect the formation of $O_2$ ($^1\Delta_g$) by an decrease in absorption at the wavelength of 355 nm [54], [55], [56]. This reaction is shown in Figure 26.

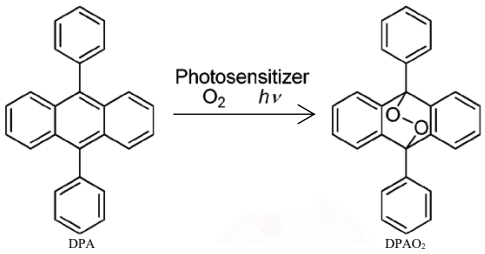


**Figure 26.** Concept of bounding of oxygen to DPA [56, p.3317]

## REACTOR DESIGN

An important parameter when performing a photochemical reaction is the productivity, which can be benchmarked with space-time yield (STY). This is the amount of product ($n$) that is formed per unit of time ($t$) and reactor volume ($V_r$) as shown in equation (8) [13], [58].

$$STY = \frac{n}{t\,V_r} \quad (8)$$

Nowadays, a photochemical reaction is usually performed in batch reactors. To reach a high productivity, the reactor can be scaled-up by an increase of the volume, catalyst concentration or light intensity. However, this leads to some disadvantages: photon transfer limitations and mass transfer limitations. First, when the reactor is irradiated with light, not all the light can irradiate the center of the reactor. This creates dark areas and slows down the reaction, hence lowering the productivity. This is illustrated in Figure 27. The phenomenon of mass transfer limitation, specifically film diffusion limitation, occurs when two different phases are used and a product of one phase has to reach the other phase to react. By mixing faster, the film gets smaller which decreases the diffusion distance. This solves the problem of mass transfer limitation [5], [12].

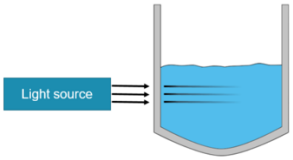


**Figure 27.** Visualization of photon transfer limitation in large batch reactors [36]

A solution for the photon transfer limitation is the use of a microreactor. These reactors consist of a small channel and have a large surface-to-volume ratio. Due to the small pathlength, the light can irradiate every single part of the reactor. This design also improves mass and heat transfer. Some disadvantages of a microreactor are the low overall energy efficiency and size of the reactor. Due to the relatively large size of the used lamps compared to the small reactor, the majority of the light leaks out of the reactor, therefore it does not contribute to the process, lowering the energy efficiency. Both disadvantages can be solved by placing more channels next to each other and above each other which creates a 3D reactor. The size of the reactor increases and photons which pass by the 2D reactor will be apprehended by the channels placed above the first row. This design is called a monolith reactor [13], [5]. The solution is shown in Figure 28.

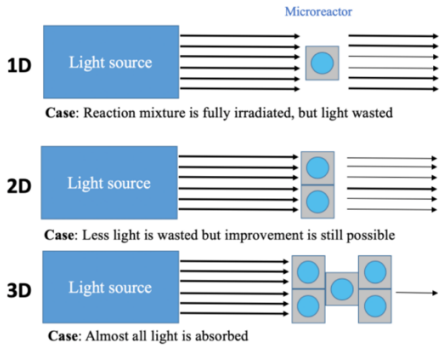


**Figure 28.** Illustration of the scale-up of microreactors [36]

The aim of a profitable process is a high productivity and conversion at the end of the process, but this is dependent on several factors. First of all, the conversion at the end of the process is equal to the average of the conversion at the end of every single channel. A distributor distributes the reaction mixture over the microchannels. Furthermore, two parameters are of uttermost importance, namely, the reaction rate and the residence time. The reaction rate depends on the amount of absorbed light, quantum yield and mass transfer limitations. The residence time depends on the throughput. The aim is that every channel has the same throughput and absorbs the same amount of light, so the conversion is the same at the end of every channel.

In the upcoming sections there will be discussed how a design of the monolith will be developed to reach the targeted conversion. First in methodology the simulation software COMSOL and the parameters which will be modified will be explained. Afterwards, the results of the simulations will be examined and discussed and finally, a conclusion will be formed.

## METHODOLOGY

To develop and to optimize the microreactor, the simulation software COMSOL is used. As mentioned before, two parameters are very important. The reaction rate is examined by the ray tracing. The throughput and residence time in each channel are investigated by computational fluid dynamics (CFD).

First, ray tracing is explained. This is a study which simulates how an electromagnetic wave reproduces through matter. Also, the interaction between particles and the light can be studied. Important is that wavelength has to be ten times smaller than the smallest body in the matter and that the model has a certain condition. This means, there has to be at least one surface that can refract and reflect a ray in a new direction. This material discontinuity creates a secondary ray.

COMSOL performs the ray tracing by solving the differential equations (9) and (10) where $\bar{z}$ is equal to the wave vector, $\omega$ is equal to the angular frequency, $\bar{q}$ is the position vector and $t$ is the time. [13], [59] .

$$\frac{d\bar{z}}{dt} = -\frac{\partial\omega}{\partial\bar{q}} \tag{9}$$

$$\frac{d\bar{q}}{dt} = \frac{\partial\omega}{\partial\bar{z}} \tag{10}$$

A light source releases a bundle of rays and the ray tracing algorithm traces its direction through the matter. These rays are defined as primary rays because they were sent directly from a source. When the primary rays hit a material discontinuity a secondary ray is reflected. Snell's law and Fresnel equations are then be used to determine the direction of the ray and its intensity or power. Depending on which surface the light hits, the other part of the light bundle is absorbed by the absorbing solution or a refracted ray reproduces itself like the incident ray [13], [59].

The complex refractive index ($k$) of the material is combined with the deposited ray power node from COMSOL to calculate how much energy is absorbed by the materials. The complex refractive index can be calculated with equation (11). This equation is a result from the combination of Lambert-Beer's law and the equation to measure the intensity of light with $\lambda$ as wavelength [13].

$$k = \frac{\varepsilon\ c\ \lambda\ ln(10)}{4\ \pi} \tag{11}$$

Second, CFD is used to analyze and solve problems from systems containing fluid flows by solving the Navier-Stokes equation. This equation consists of two partial differentials, the conservation of momentum, equation (12) and the conservation of mass, equation (13). These describe the flow of a fluid with $\bar{v}$ is equal to the speed vector, $t$ is equal to the time, $p$ is equal to the pressure and $\bar{g}$ is equal to the gravity vector. The fluid is incompressible and Newtonian [60], [61].

$$\rho \frac{d\bar{v}}{dt} = -\nabla p + \mu \nabla^2 \bar{v} + \rho \bar{g} \quad (12)$$

$$\nabla \bar{v} = 0 \quad (13)$$

The flow regime can be determined with Reynolds number, $N_{Re}$, equation (14), with $D$ is equal to the characteristic length of the channel, $v$ is equal to the speed of the flow, $\rho$ is equal to the density and $\mu$ is equal to the viscosity. If $N_{Re}$ is smaller than 2100, the flow is laminar [60], [61].

$$N_{Re} = \frac{D\ v\ \rho}{\mu} \quad (14)$$

Due to the low velocity and the small characteristic length of the channels in the monolith, the flow can be considered as laminar.

To perform CFD simulations, the finite analytic method (FAM) is performed to solve the partial differential equations. In this method the problem is solved by dividing the system into smaller elements, finite elements, which is achieved by constructing a mesh. A system of algebraic equations is formulated from where COMSOL calculates the velocity, pressure and throughput [60], [62], [63].

Different monolith reactors are validated with a refraction index of 1.5. The absorbent, DPA, pumped through the reactor has a refraction index of 1,333 and is brought into the reactor with a concentration of 2 mM. It has a specific absorbent coefficient of 9000 $m^2$/mol [64].

## Results and Discussion

### Ray tracing

The reactor is built out of multiple unit cells. This is a repeating unit which cannot be divided into other units. Several unit cells together built the monolith reactor. A sample design of a reactor is shown in Figure 29. This reactor consists of unit cells with two rows of channels where the channel in the next row is placed in the center of the previous row.

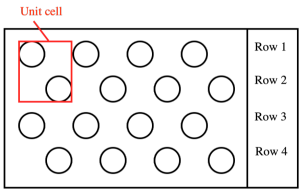


**Figure 29.** A sample design of a reactor consisting of two unit cells above each other and four next to each other

During the experiments, various parameters are changed, and each design is validated. The homogeneity of the light absorption in each reactor is investigated by calculating the relative SD (RSD) of the light absorption through each channel. Also, the percentage of light absorbed by the monolith reactor and the light balance are calculated. The light balance gives information about the ratio of standardized light absorbed by the reactor and the standardized light that was emitted. This parameter is calculated to control the amount of light lost by the simulation. Desired is a light balance of 1 [13].

The first parameter modified is the power of the lamp. Table 16 gives information of the influence of this parameter. There can be concluded that when the power of the lamp increases, the light absorbed by the reactor also increases. The percentage of light absorbed, RSD and the light balance are constant. This means that the power has no influence on the homogeneity and the percentage of light absorbed by the reactor but only on the total amount of light absorbed. The light balance is around 1 which is good.

**Table 16.** The influence of the power of the lamp in a 16x2 monolith reactor with a channel diameter of 3 mm

| Power (W) | Light absorbed (W) | Light absorbed (%) | RSD (%) | Light balance |
|---|---|---|---|---|
| 50 | 42.36 | 84.72 | 6.92 | 1.013 |
| 100 | 84.72 | 84.72 | 6.92 | 1.013 |
| 200 | 169.45 | 84.73 | 6.92 | 1.013 |
| 500 | 423.65 | 84.73 | 6.92 | 1.013 |
| 750 | 635.48 | 84.73 | 6.92 | 1.013 |
| 1000 | 847.31 | 84.73 | 6.92 | 1.013 |

Next, the number of rows, the diameter of the channels and the number of channels per row are modified. The results of the different monolith reactor designs are shown in Figure 31 and Figure 32.

First, the influence of the number of rows is examined. Figure 31a shows that the RSD increases when the number of rows increases which is undesired. This figure also shows that the percentage of light absorbed remains constant with an increasing number of rows which is also undesired. The light balance, Figure 31b, decreases with the number of rows. When the percentage of light absorbed per row is studied, shown in Figure 30, these results can be explained.

The reactor design in Figure 30a shows that the amount of light absorbed in the first row is 10 % lower than in the second row. This is not a significant difference, therefore a low RSD is obtained. Then, in the reactor design shown in Figure 30b, the amount of light in the first two rows is clearly more than in the last two rows. This results in a higher RSD and by the low amount of light absorbed in the last two rows, the percentage of light absorbed is not change much toward the reactor with one row unit cells. Last, the same results as the reactor with two rows unit cells are observed in the reactor shown in Figure 30c. The first two rows absorb significantly more light than the next four rows which results in a further increase of the RSD. Also, by the low amount of light absorbed in the last two unit cells, the percentage of light absorbed is constant. The decrease of light balance can be explained by the low amount of light absorbed at the lower wall of the reactor.

This decreases the light absorbed by the reactor which leads to a decrease of the light balance.

The homogeneity, in a reactor consisting of multiple unit cells above each other, can be improved by lowering the concentration of absorbent. Less light will be absorbed in the first rows so more light will go through to the next rows [13].

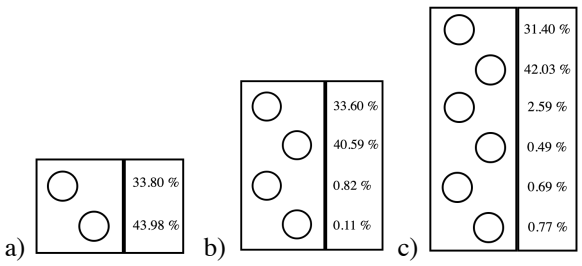


**Figure 30.** Illustration of the percentage of light absorbed per row channels for the reactor designs: a) 16x2, b) 16x4 and c) 16x6 with a channel diameter of 2 mm

After the examination of the influence of the number of rows, the influence of the diameter of the channels and of the number of channels per row are studied. The results are shown in Figure 32. First of all, a diameter of 2 mm shows abnormal results. These results are not taken into account in the discussions.

After analyzing the results of an increasing diameter, there can be concluded that the percentage of light absorbed increases, Figure 32a. This can be explained by an increase of the surface that can absorb light. For the light balance, Figure 32b, can be concluded that no significant difference between the different diameters is observed. The RSD, Figure 32a, does not change much with an increase of the diameter. This means that the homogeneity in each reactor is approximately the same. When the diameter increases, the influence of mass transfer limitation also increases. So, when working with an immobilized catalyst it is important to choose a reactor with a smaller diameter [13].

Last, the number of channels per row is changed. Here, as expected, the percentage of light absorbed, Figure 32a, raises with the number of channels. This is caused by an increase of the surface that can absorb light. Also, the light balance, Figure 32b, grows with the number of channels. The RSD, Figure 32a, is the lowest for a reactor with the design 16x2 which means that the homogeneity is the best in this reactor.

Overall, there can be concluded that a reactor consisting of one unit cells, two rows of channels, gives the best results. This design is used for the next experiments.

### COMPUTATIONAL FLUID DYNAMICS

Also, for this part of the simulations, various parameters are changed, and each design is validated. The homogeneity of the throughput in each reactor is investigated by calculating the RSD of the throughput through each channel [64].

First, the influence of the inlet diameter of the distributor is examined. The results of these simulations are shown in Figure 33. There can be concluded that an inlet diameter of 1 mm has the lowest RSD followed by an inlet diameter of 4 mm. This means that the homogeneity of the throughput in these reactors are the highest. Also, the inlet diameter affects the inlet throughput. The throughput can be measured by equation (15). This equation says that the throughput ($q\nu$) is equal to the flow area ($r^2 \cdot \pi$ ) times the velocity ($\nu$) and so, as the diameter ($r \cdot 2$) of the inlet channel increases, the throughput increases. For further simulations, an inlet diameter of 4 mm is used.

$$q\nu = r^2 \, \pi \;\; \nu \tag{15}$$

Second, the inlet velocity is modified. As mentioned in the last equation, the throughput increases with the velocity. So, the highest throughput is reached by the highest velocity. The results of the homogeneity are shown in Figure 34. These results illustrate that the RSD increases with the inlet velocity. This can be explained by Newton's laws. The mixture enters the reactor with a specific velocity and is distributed over the channels. No force has to be applied to the mixture to bring it in the central channels. The velocity is not changed. To bring the mixture to the outer channels, a force has to be applied which leads to a delay and a lower velocity. The influence of this phenomenon increases when the velocity increases because a bigger force has to be applied. This means that the homogeneity decreases with an increase of the velocity causing an increase of the RSD.

Last, the influence of the channel diameter and the number of channels are examined. The results are shown in Figure 35. There can be noted that the RSD, Figure 35a, increases with the diameter of the channels and with the number of channels. This can also be declared by Newton's laws. First, when the diameter increases the dimensions of the reactor raises. This means a higher force has to be applied on the mixture to bring it to the outer channels. So, the velocity decreases in the outer channels in contrast to the central channels which leads to a lower homogeneity and a higher RSD. This is also the case when the number of channels increases, Figure 35a. When the dimensions of the reactor increase, a higher force has to be applied to the mixture to bring it to the outer channels and the velocity decreases in contrast to the central channels. So, the RSD increases.

In this case, also the influence on the inlet throughput, Figure 35b, is studied but this is overall constant. Only the inlet diameter and the inlet velocity have a big influence on the inlet throughput.

### PHOTOCHEMICAL SPACE-TIME YIELD

Out of the previous results, the STY and the photochemical space-time yield (PSTY) can be measured to evaluate the productivity and the energy efficiency of the monolith reactor. The last parameter reflects the amount of product

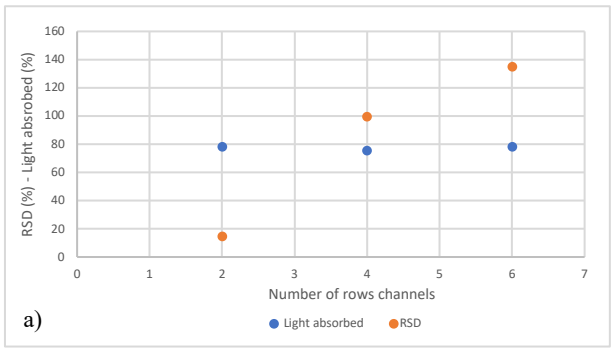


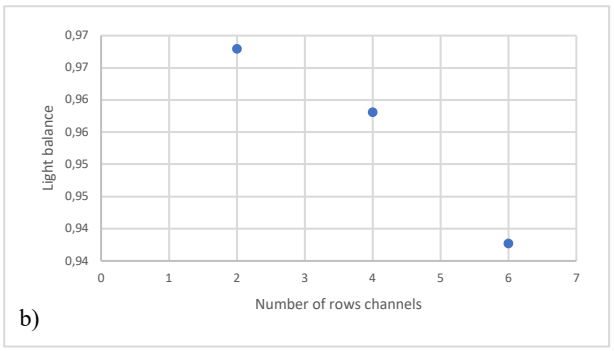


**Figure 31.** Illustration of the influence of the number of rows: a) on the RSD and percent light absorbed and b) on the light balance of a 16x2 reactor with a channel diameter of 2 mm

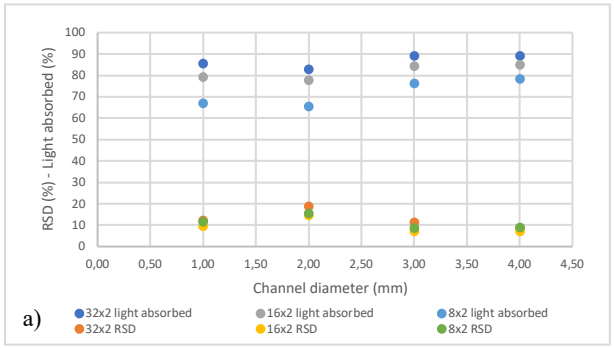


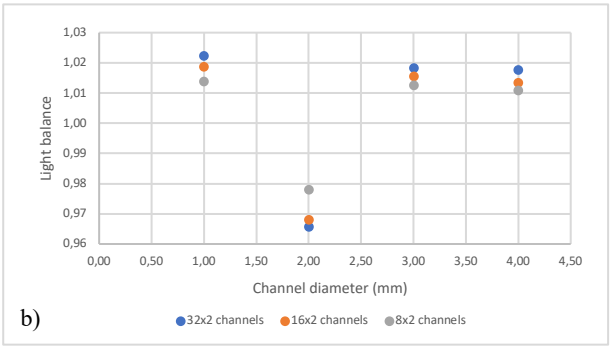


**Figure 32.** Illustration of the influence of the channel diameter and the number of channels per row: a) on the RSD and percent light absorbed and b) on the light balance

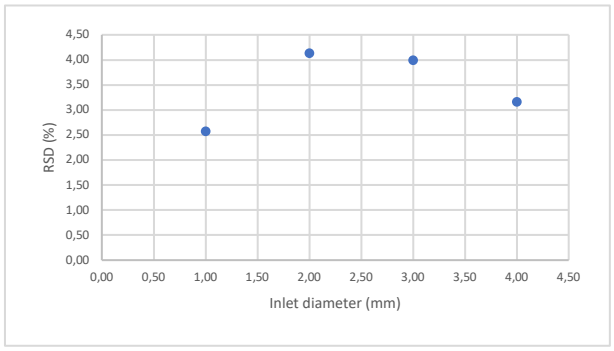


**Figure 33.** Illustration of the influence of the inlet diameter on the RSD of an 8x2 reactor with a channel diameter of 2 mm

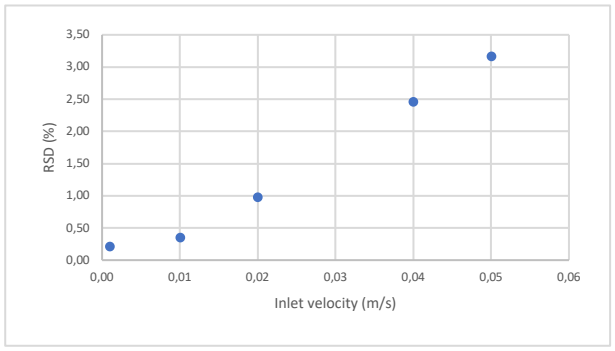


**Figure 34.** Illustration of the influence of the inlet velocity on the RSD of an 8x2 reactor with an inlet diameter of 4 mm and a channel diameter of 2 mm

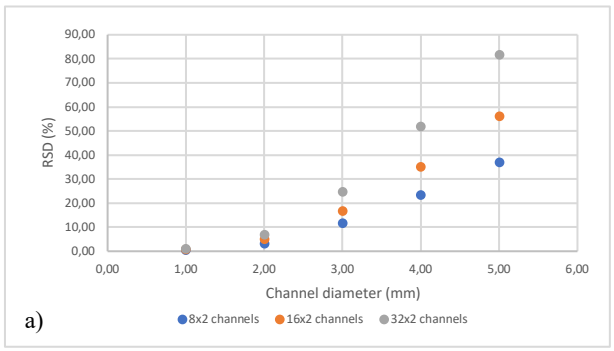


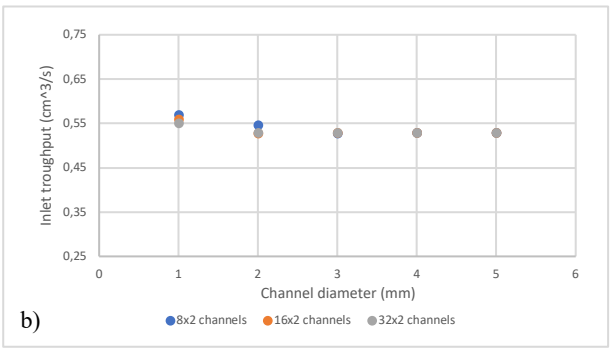


**Figure 35.** Illustration the influence of the channel diameter and the number of channels per row: a) on the RSD and b) on the inlet throughput

produced by a volumetric specific yield per lamp power and unit of time [13], [58].

Using the results of the ray tracing, the amount of product generated per unit of time can be calculated by equation (16) for each channel. $P_{abs}$ is equal to the light absorbed by the mixture, $\nu_L$ is the speed of light, $h$ is equal to Planck's constant and $N_A$ is equal to Avogadro's number [58].

$$\frac{\#\ product\ generated}{s} = \frac{P_{abs}\ \lambda\ \Phi}{\nu_L\ h\ N_A} \tag{16}$$

Next, the residence time ($\tau$), in each channel ($V_s$), can be measured out of the results of CFD by equation (17) [58].

$$\tau = \frac{V_s}{q\nu} \tag{17}$$

Then, the amount of product ($n$) formed per channel can be calculated by multiplying equation (16) by equation (17). To measure the STY, the average of the residence time and the total amount of product formed have to be calculated first. With these data the STY of the reactor can be calculated according to equation 8 [58].

Last, to calculate the PSTY with equation (19), the standardized lamp power ($LP$) has to be measured by equation (18) where $P$ is equal to the power of the lamp [58].

$$LP = P\ \frac{1\ m^3}{Vr} \tag{18}$$

$$PSTY = \frac{STY}{LP} \tag{19}$$

Table 17 shows the results of the calculations of the PSTY for monolith reactors with an inlet diameter of 4 mm and a velocity of 0.001 m/s. There can be concluded that the PSTY is the highest for reactors with the largest diameter or with the highest number of channels. This can be explained by the larger volume of the reactor so, photons are longer in contact with the mixture. When the velocity increases, the amount of product formed ($mol$) decreases due to a decrease residence time. But this has no influence on the STY and PSTY. The STY decreases with an increase of the channel diameter which means that the productivity decreases. So, the best reactor is a reactor with small channel diameters and a high absorption rate. Furthermore, a small channel diameter decreases mass transfer limitations [13].

## CONCLUSION

During the experiments, different parameters were modified to optimize a monolith for photochemical reactions. Different monolith reactors were used because of its large surface-to-volume ratio and its high energy efficiency. The PSTY was measured to benchmark these different reactor designs so that it could be compared. While studying the results of the ray tracing, it was preferred to use a design consisting of one unit cells for further experiments due to its high irradiance homogeneity. By an increase of the surface of the reactor, the percentage of light absorbed increased. Out of the results of CFD, there was concluded that an inlet diameter of 4 mm had to be used for further experiment because of its low RSD and its effect on the inlet throughput. Next PSTY was calculated and it concluded that a larger volume of the reactor results in a higher PSTY. This is due the longer time that the photons were traveling through the mixture. The STY decreased by a larger volume, so it is important to choose the reactor with the highest PSTY and highest STY. It is also important to remember the mass transfer limitation phenomenon. When using an immobilized catalyst, it is recommended to choose a reactor with a small channel diameter because it lowers the mass transfer limitation.

## FUTURE

The next step in the process of the development of a productive and energy efficient monolith reactor is an experimental setup of the best reactors. The reactors will be printed by a 3D-printer and the same parameters will have to be validated to evaluate the reactor design. Further, new simulations have to be run to optimize the reactor design or to develop a more productive and energy efficient reactor.


## ACKNOWLEDGMENTS

Thanks to ing. Mathias Jacobs and Prof. dr. ir. Mumin Enis Leblebici to supervise this article.


**Table 17.** Summary of the results to measure the PSTY of different reactor designs

| Reactor design | Diameter channel (m) | Volume reactor ($m^3$) | n (mol) | τ (s) | STY (mol $s^{-1}$ $m^{-3}$) | LP (W $m^{-3}$) | PSTY (mol $s^{-1}$ $m^{-3}$ $W^{-1}$) |
|---|---|---|---|---|---|---|---|
| 8x2 | 0.001 | $1.88 \times 10^{-6}$ | 1.06 | 179.48 | 3124.93 | 1494663853.50 | $2.09 \times 10^{-6}$ |
| 8x2 | 0.002 | $7.54 \times 10^{-6}$ | 2.16 | 748.93 | 381.92 | 180243763.27 | $2.12 \times 10^{-6}$ |
| 8x2 | 0.003 | $1.70 \times 10^{-5}$ | 3.89 | 1739.37 | 131.96 | 55283693.68 | $2.39 \times 10^{-6}$ |
| 8x2 | 0.004 | $3.01 \times 10^{-5}$ | 5.31 | 3078.66 | 57.21 | 23286799.69 | $2.46 \times 10^{-6}$ |
| 16x2 | 0.001 | $3.77 \times 10^{-6}$ | 1.35 | 1.35 | 979.29 | 397482287.69 | $2.46 \times 10^{-6}$ |
| 16x2 | 0.002 | $1.51 \times 10^{-5}$ | 2.81 | 2.81 | 120.51 | 47196005.84 | $2.55 \times 10^{-6}$ |
| 16x2 | 0.003 | $3.39 \times 10^{-5}$ | 4.55 | 4.55 | 38.70 | 14621583.81 | $2.65 \times 10^{-6}$ |
| 16x2 | 0.004 | $6.03 \times 10^{-5}$ | 6.07 | 6.07 | 16.41 | 6175922.41 | $2.66 \times 10^{-6}$ |
| 32x2 | 0.001 | $7.54 \times 10^{-6}$ | 1.53 | 1.53 | 272.95 | 102768906.58 | $2.66 \times 10^{-6}$ |
| 32x2 | 0.002 | $3.01 \times 10^{-5}$ | 3.06 | 3.06 | 33.01 | 12134900.64 | $2.72 \times 10^{-6}$ |
| 32x2 | 0.003 | $6.78 \times 10^{-5}$ | 4.91 | 4.91 | 10.51 | 3791271.82 | $2.77 \times 10^{-6}$ |
| 32x2 | 0.004 | $1.21 \times 10^{-4}$ | 6.50 | 6.50 | 4.44 | 1598449.86 | $2.78 \times 10^{-6}$ |

# References


[1] "LAB4U - (BIO-)CHEMISCHE PROCESTECHNOLOGIE," *KULeuven*, 2020. [Online]. Available: https://iiw.kuleuven.be/onderzoek/lab4U. [Accessed: 15-Mar-2020].

[2] Y. Zhang, S. U. Geißen, and C. Gal, "Carbamazepine and diclofenac: Removal in wastewater treatment plants and occurrence in water bodies," *Chemosphere*, vol. 73, no. 8, pp. 1151–1161, 2008, doi: 10.1016/j.chemosphere.2008.07.086.

[3] "Waterzuivering," *aquafin*, 2020. [Online]. Available: https://www.aquafin.be/nl-be/particulieren/waterzuivering. [Accessed: 13-Mar-2020].

[4] M. E. Leblebici, "Design, modelling and benchmarking of photoreactors and separation processes for waste treatment and purification," no. May, 2017.

[5] D. Cambié, C. Bottecchia, N. J. W. Straathof, V. Hessel, and T. Noël, "Applications of Continuous-Flow Photochemistry in Organic Synthesis, Material Science, and Water Treatment," *Chem. Rev.*, vol. 116, no. 17, pp. 10276–10341, 2016, doi: 10.1021/acs.chemrev.5b00707.

[6] N. Hashim, "Visible Light Driven Photocatalysis for Degradation of Diclofenac," □□□□□ □□□□□□□, no. April, 2016.

[7] VMM, "Medicijnen in de waterketen. Resultaten verkennend onderzoek in de periode 2014-2016," 2017.

[8] G. Tchobanoglous, F. Burton, and H. D. Stensel, "Wastewater engineering: An Overview," *Wastewater Eng. Treat. Reuse*, pp. 1–24, 1991, doi: 10.1016/0309-1708(80)90067-6.

[9] A. Ziylan and N. H. Ince, "The occurrence and fate of anti-inflammatory and analgesic pharmaceuticals in sewage and fresh water: Treatability by conventional and non-conventional processes," *J. Hazard. Mater.*, vol. 187, no. 1–3, pp. 24–36, 2011, doi: 10.1016/j.jhazmat.2011.01.057.

[10] L. Braeken, *Milieutechnologie en veiligheid in chemische installaties*. Diepenbeek: UHasselt.

[11] T. Jeltes, "Chemie met zonne-energie," *Cursor*, 2015. [Online]. Available: https://www.cursor.tue.nl/nieuws/2015/juni/chemie-met-zonne-energie/. [Accessed: 01-Sep-2019].

[12] M. E. Leblebici, *Industriële (bio)chemische processen en corrosie*. Diepenbeek.

[13] M. Jacobs, E. Kayahan, L. C. J. Thomassen, S. Kuhn, and M. E. Leblebici, "First generation of translucent monoliths for photochemical applications," *J. Adv. Manuf. Process.*, vol. n/a, no. n/a, p. e10047, 2020, doi: 10.1002/amp2.10047.

[14] L. Maes, *Basischemie*. Diepenbeek: KHLim.

[15] E. Wieërs and S. Wouters, *Fysica voor industrieel ingenieurs, schakelprogramma*, Second. Diepenbeek: UHasselt/KULeuven, 2014.

[16] "Light," *Astronomy Education at the University of Nebraska-Lincoln*. [Online]. Available: https://astro.unl.edu/naap/hydrogen/light.html. [Accessed: 06-Mar-2020].

[17] "Electromagnetic Radiation," *Byju's*, 2020. [Online]. Available: https://byjus.com/physics/electromagnetic-radiation/. [Accessed: 04-Sep-2019].

[18] L. Leijnen, A. Creemers, H. Kees, M. Vanhecke, and E. Gubbelmans, *Instrumentele analyse fotometrie en chemische dataverwerking*. Diepenbeek: UCLL.

[19] "Stark-Einstein law," *Oxford Reference*. [Online]. Available: https://www.oxfordreference.com/view/10.1093/oi/authority.20110803100528576. [Accessed: 05-Sep-2020].

[20] C. P. Schaller, "14.7: Fluorescence and Phosphorescence," 202AD. [Online]. Available: https://chem.libretexts.org/Bookshelves/Physical_and_Theoretical_Chemistry_Textbook_Maps/Map%3A_Physical_Chemistry_for_the_Biosciences_(Chang)/14%3A_Spectroscopy/14.7%3A_Fluorescence_and_Phosphorescence. [Accessed: 25-Mar-2020].

[21] D. Kanakaraju, C. A. Motti, B. D. Glass, and M. Oelgemöller, "Photolysis and TiO2-catalysed degradation of diclofenac in surface and drinking water using circulating batch photoreactors," *Environ. Chem.*, vol. 11, no. 1, pp. 51–62, 2014, doi: 10.1071/EN13098.

[22] "Super Efficient LEDs," 2020. [Online]. Available: https://www.physicscentral.com/explore/action/led.cfm. [Accessed: 18-Apr-2020].

[23] "Efficiency of LEDs: The highest luminous efficacy of a white LED," 2016. [Online]. Available: https://www.dial.de/en/blog/article/efficiency-of-ledsthe-highest-luminous-efficacy-of-a-white-led/. [Accessed: 18-Apr-2020].

[24] H. C. Chen and G. Y. Wu, "Investigation of irradiance efficiency for LED phototherapy with different arrays," *Opt. Commun.*, vol. 283, no. 24, pp. 4882–4886, 2010, doi: 10.1016/j.optcom.2010.07.055.

[25] "KATALYSATOREN: EEN DUWTJE IN DE RUG," *Scheikunde voor beginners*. [Online]. Available: https://voorbeginners.info/scheikunde/katalysatoren.htm. [Accessed: 07-Sep-2019].

[26] S. Sakthivel, M. V. Shankar, M. Palanichamy, B. Arabindoo, D. W. Bahnemann, and V. Murugesan, "Enhancement of photocatalytic activity by metal deposition: Characterisation and photonic efficiency of Pt, Au and Pd deposited on TiO 2 catalyst," *Water Res.*, vol. 38, no. 13, pp. 3001–3008, 2004, doi: 10.1016/j.watres.2004.04.046.

[27] Z. Du, C. Feng, Q. Li, Y. Zhao, and X. Tai, "Photodegradation of NPE-10 surfactant by Au-doped nano-TiO2," *Colloids Surfaces A Physicochem. Eng. Asp.*, vol. 315, no. 1–3, pp. 254–258, 2008, doi: 10.1016/j.colsurfa.2007.08.028.

[28] S. Y. Lee and S. J. Park, "TiO2 photocatalyst for water treatment applications," *J. Ind. Eng. Chem.*, vol. 19, no. 6, pp. 1761–1769, 2013, doi: 10.1016/j.jiec.2013.07.012.

[29] D. Kanakaraju, B. D. Glass, and M. Oelgemöller, "Titanium dioxide photocatalysis for pharmaceutical wastewater treatment," *Environ. Chem. Lett.*, vol. 12, no. 1, pp. 27–47, 2014, doi: 10.1007/s10311-013-0428-0.

[30] C. Martínez, M. Canle L., M. I. Fernández, J. A. Santaballa, and J. Faria, "Aqueous degradation of diclofenac by heterogeneous photocatalysis using nanostructured materials," *Appl. Catal. B Environ.*, vol. 107, no. 1–2, pp. 110–118, 2011, doi: 10.1016/j.apcatb.2011.07.003.

[31] M. V. Bagal and P. R. Gogate, "Degradation of diclofenac sodium using combined processes based on hydrodynamic cavitation and heterogeneous photocatalysis," *Ultrason. Sonochem.*, vol. 21, no. 3, pp. 1035–1043, 2014, doi: 10.1016/j.ultsonch.2013.10.020.

[32] N. Zhang, J. M. Li, G. G. Liu, X. L. Chen, and K. Jiang, "Photodegradation of diclofenac in aqueous solution by simulated sunlight irradiation: Kinetics, thermodynamics and pathways," *Water Sci. Technol.*, vol. 75, no. 9, pp. 2163–2170, 2017, doi: 10.2166/wst.2017.075.

[33] M. Oelgemoeller, "Highlights of Photochemical Reactions in Microflow Reactors," *Chem. Eng. Technol.*, vol. 35, no. 7, pp. 1144–1152, 2012, doi: 10.1002/ceat.201200009.

[34] H. Yamaguchi, T. Honda, and M. Miyazaki, “Application of enzyme-immobilization technique for microflow reactor,” *J. Flow Chem.*, vol. 6, no. 1, pp. 13–17, 2016, doi: 10.1556/1846.2015.00039.

[35] R. Gorges, S. Meyer, and G. Kreisel, “Photocatalysis in microreactors,” *J. Photochem. Photobiol. A Chem.*, vol. 167, no. 2–3, pp. 95–99, 2004, doi: 10.1016/j.jphotochem.2004.04.004.

[36] M. Jacobs, K. Emine, and M. E. Leblebici, “First generation of translucent monoliths with 3D-printing for photocatalysis in the visible light region,” in *UCRA*.

[37] A. Šalić, A. Tušek, and B. Zelić, “Application of microreactors in medicine and biomedicine,” *J. Appl. Biomed.*, vol. 10, no. 3, pp. 137–153, 2012, doi: 10.2478/v10136-012-0011-1.

[38] “Principle of 3d printing-Fused Deposition Modeling(FDM),” *Tanerxun*. [Online]. Available: https://www.tanerxun.com/fused-deposition-modeling-principle/.html. [Accessed: 26-Mar-2020].

[39] “Introduction to SLA 3D Printing,” *3D HUBS*. [Online]. Available: https://www.3dhubs.com/knowledge-base/introduction-sla-3d-printing/#what. [Accessed: 26-Mar-2020].

[40] “Spectrophotmetry,” *Chemistry LibreTexts*, 2019. [Online]. Available: https://chem.libretexts.org/Bookshelves/Physical_and_Theoretical_Chemistry_Textbook_Maps/Supplemental_Modules_(Physical_and_Theoretical_Chemistry)/Kinetics/Reaction_Rates/Experimental_Determination_of_Kinetcs/Spectrophotometry. [Accessed: 26-Mar-2020].

[41] G. Raymaekers, *Analytische Chemie III*. Diepenbeek.

[42] A. Sagar, “High-Performance Liquid Chromatography (HPLC),” *Online Microbiology Notes*, 2020. [Online]. Available: https://microbenotes.com/high-performance-liquid-chromatography-hplc/. [Accessed: 26-Mar-2020].

[43] U. Latif and F. L. Dickert, “Chemical Oxygen Demand,” pp. 719–728, 2015, doi: 10.1007/978-1-4939-1301-5_1.

[44] L. A. Pérez-Estrada *et al.*, “Decomposition of diclofenac by solar driven photocatalysis at pilot plant scale,” *Catal. Today*, vol. 101, no. 3-4 SPEC. ISS., pp. 219–226, 2005, doi: 10.1016/j.cattod.2005.03.013.

[45] M. I. Cabrera, O. M. Alfano, and A. E. Cassano, “Absorption and scattering coefficients of titanium dioxide participate suspensions in water,” *J. Phys. Chem.*, vol. 100, no. 51, pp. 20043–20050, 1996, doi: 10.1021/jp962095q.

[46] “Study Notes: Deviations from Beer’s Law.” [Online]. Available: http://simulab.ltt.com.au/5/Laboratory/StudyNotes/snDeviatFromBeerLaw.htm. [Accessed: 06-Apr-2020].

[47] J. Tittor and D. Oesterhelt, “The quantum yield of bacteriorhodopsin,” *FEBS Lett.*, vol. 263, no. 2, pp. 269–273, 1990, doi: 10.1016/0014-5793(90)81390-A.

[48] A. Krieger-Liszkay, “Singlet oxygen production in photosynthesis,” *J. Exp. Bot.*, vol. 56, no. 411, pp. 337–346, 2005, doi: 10.1093/jxb/erh237.

[49] M. C. DeRosa and R. J. Crutchley, “Photosensitized singlet oxygen and its applications,” *Coord. Chem. Rev.*, vol. 233–234, pp. 351–371, 2002, doi: 10.1016/S0010-8545(02)00034-6.

[50] H. J. Reich, “Singlet Oxygen,” 2019. [Online]. Available: https://www.chem.wisc.edu/areas/reich/chem547/2-redox%7B26%7D.htm. [Accessed: 24-Apr-2020].

[51] L. V. Lutkus, S. S. Rickenbach, and T. M. McCormick, “Singlet oxygen quantum yields determined

by oxygen consumption," *J. Photochem. Photobiol. A Chem.*, vol. 378, no. April, pp. 131–135, 2019, doi: 10.1016/j.jphotochem.2019.04.029.

[52] W. M. Sharman, C. M. Allen, and J. E. Van Lier, "Photodynamic therapeutics: Basic principles and clinical applications," *Drug Discov. Today*, vol. 4, no. 11, pp. 507–517, 1999, doi: 10.1016/S1359-6446(99)01412-9.

[53] 李步洪 Buhong Li, 林慧韫 Huiyun Lin, 陈德福 Defu Chen, 王敏 Min Wang, and 谢树森 Shusen Xie, "Detection system for singlet oxygen luminescence in photodynamic therapy," *Chinese Opt. Lett.*, vol. 8, no. 1, pp. 86–88, 2010, doi: 10.3788/col20100801.0086.

[54] L. Slavětínská, J. Mosinger, and P. Kubát, "Supramolecular carriers of singlet oxygen: Photosensitized formation and thermal decomposition of endoperoxides in the presence of cyclodextrins," *J. Photochem. Photobiol. A Chem.*, vol. 195, no. 1, pp. 1–9, 2008, doi: 10.1016/j.jphotochem.2007.09.007.

[55] W. Fudickar and T. Linker, "Release of Singlet Oxygen from Aromatic Endoperoxides by Chemical Triggers," *Angew. Chemie - Int. Ed.*, vol. 57, no. 39, pp. 12971–12975, 2018, doi: 10.1002/anie.201806881.

[56] N. Umezawa, K. Tanaka, Y. Urano, K. Kikuchi, T. Higuchi, and T. Nagano, "Novel fluorescent probes for singlet oxygen," *Angew. Chemie - Int. Ed.*, vol. 38, no. 19, pp. 2899–2901, 1999, doi: 10.1002/(SICI)1521-3773(19991004)38:19<2899::AID-ANIE2899>3.0.CO;2-M.

[57] S. Martins, J. P. S. Farinha, C. Baleizão, and M. N. Berberan-Santos, "Controlled release of singlet oxygen using diphenylanthracene functionalized polymer nanoparticles," *Chem. Commun.*, vol. 50, no. 25, pp. 3317–3320, 2014, doi: 10.1039/c3cc48293f.

[58] M. E. Leblebici, G. D. Stefanidis, and T. Van Gerven, "Comparison of photocatalytic space-time yields of 12 reactor designs for wastewater treatment," *Chem. Eng. Process. Process Intensif.*, vol. 97, pp. 106–111, 2015, doi: 10.1016/j.cep.2015.09.009.

[59] Comsol, *COMSOL - Ray Optics Module User's Guide [Guide]*, Comsol 5.4. U.S.: Comsol.

[60] Comsol, *COMSOL - CFD Module User's Guide [Guide]*, COMSOL 5.4. U.S.: Comsol.

[61] B. Baeten, W. Deferme, and F. Rogiers, *Fluïdummechanica en thermodynamica [source]*. Diepenbeek: UHasselt/KULeuven.

[62] W. Lin, Y. Haik, R. Bernatz, and C. J. Chen, "Finite analytic method and its applications: A review," *Dyn. Atmos. Ocean.*, vol. 27, no. 1–4, pp. 17–33, 1998, doi: 10.1016/s0377-0265(97)00024-9.

[63] Z. Zhang *et al.*, "Finite analytic method for modeling variably saturated flows," *Sci. Total Environ.*, vol. 621, pp. 1151–1162, 2018, doi: 10.1016/j.scitotenv.2017.10.112.

[64] F. Zhao *et al.*, "Scale-up of a Luminescent Solar Concentrator-Based Photomicroreactor via Numbering-up," *ACS Sustain. Chem. Eng.*, vol. 6, no. 1, pp. 422–429, 2018, doi: 10.1021/acssuschemeng.7b02687.